Available online at www.CivileJournal.org

Civil Engineering Journal

(E-ISSN: 2476-3055; ISSN: 2676-6957)

Vol. 12, No. 06, June, 2026

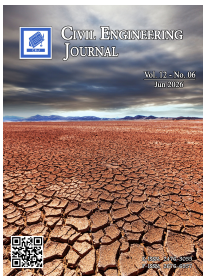

Dynamic Proportionality of Inertia and Reaction Forces in CFRP-Strengthened L-Shaped RC Beams under Impact Loading

Enas M. Mouwainea [1*], Ahlam A. Abbood [1], Nazar Oukaili [1]

[1] *Department of Civil Engineering, University of Baghdad, Baghdad, Iraq.*

Received 17 March 2026; Revised 11 May 2026; Accepted 15 May 2026; Published 01 June 2026

Abstract

This study computationally investigates to examine the impacts of repeated loading on L-shaped spandrel beams made of reinforced concrete, which were strengthened by externally bonded carbon fiber reinforced plastic sheets. The object of the research is to evaluate the following three aspects of structural behavior: degradation of reaction forces, evolution of inertia forces, and residual performance. Ayad and Oukaili's experimental impact-loading program, which featured midspan drop-weight loading on RC spandrel beams before and after strengthening, was used to validate a comprehensive three-dimensional finite element model created in ABAQUS. A sequence of 25 impacts before and 25 impacts after CFRP application was simulated to trace impact force, reaction force, inertia force, midspan deflection, and damage progression. Because of cumulative stiffness deterioration, the peak impact force in the unstrengthened beams reduced by 45%, the reaction force decreased by 54.7–57.3%, and the inertia force increased by 237.5–1090%. The peak impact force decline was limited to 31.8% with CFRP strengthening, whereas the reaction force reduction varied from 36.9% to 39%. In comparison to the much greater amplification seen prior to strengthening, the rise in inertia forces was also much reduced, staying between 114.6 and 122.2%. Additionally, there was a 19.2–23.2% decrease in the midspan deflection at the 25th impact. After 25 impacts, CFRP-strengthened beams maintained 68.3–70% of their initial capacity, but unstrengthened beams only maintained 56.2–60.1%, according to the residual performance index (RPI), which showed a notable improvement. Concrete had saturated tensile cracking prior to strengthening, according to damage analysis, but matrix microcracking (HSNMTCRT) without fiber tensile damage (DAMAGEFT) dominated post-retrofit behavior, indicating the efficient confinement and energy-dissipating function of CFRP. These results extend the previous experimental interpretation by quantifying repeated-impact trends in reaction and inertia forces, and show that externally bonded CFRP sheets improve the service-life performance of reinforced concrete ledged beams by enhancing stiffness retention, energy dissipation, inertial stability, and damage control.

Keywords: Ledged Beam; CFRP Strengthening; Structural Response; Repeated Impacts; Damage Progression.

1. Introduction

In both monolithic and precast concrete buildings, reinforced or prestressed spandrel beams are often important structural elements [1]. A spandrel beam is an exterior member that supports slabs, joists, or beams on one side. Reinforced concrete spandrel beams are often preferred over prestressed beams in applications requiring complex architectural details or high-quality surface finishing and are usually used across various building types and structural layouts. One common application is as simple-span ledge beams that support prestressed deck components in parking structures, where they also function as perimeter barriers capable of resisting impact loads. Spandrel beams reduce the need for additional columns and lower construction costs because they allow for increased span lengths within the limits

* Corresponding author: enas.m@coeng.uobaghdad.edu.iq

https://doi.org/10.28991/CEJ-2026-012-06-07

of permissible bending and deflection. As span lengths increase, the depth of the beam is improved to balance the structural requirements with transportation load limits and material efficiency [2]. The typical configuration for the spandrel beam is shown in Figure 1.

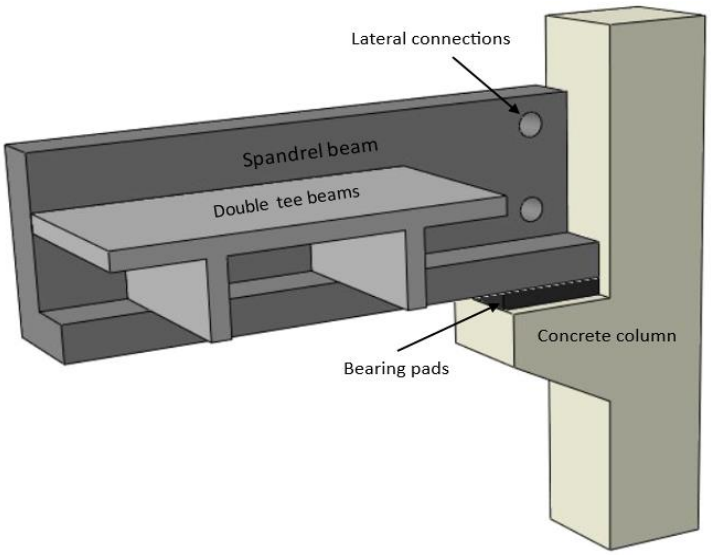

Figure 1. Typical configuration of spandrel beam

Research on precast prestressed concrete spandrels has so far typically focused on strength and design parts, paying special consideration to how they respond to combined shear, torsion, and bending motions [3]. Nevertheless, there is a significant gap in the available literature about the impact performance of spandrel beams because comparatively little experimental study has been done on this topic.

In 1983, Ali [4] studied eighteen samples with different loading types, concrete strengths, and reinforced ratios in order to study the performance and strength of reinforced concrete floor spandrel beam structures. According to the study, samplings without torsional reinforcement exhibited up to 20% less strength, whereas increasing longitudinal and transverse reinforcement enhanced torsional capacity and ductility by about 25–30%. Analytical predictions and test findings agreed within 10% to 15%. Ali concluded that post-cracking design procedures offer more accurate and cost-effective forecasts, with the minimum amount of torsional reinforcement necessary to ensure sufficient ductility and avoid brittle failure.

Lucier et al. (2007) [5] tested long and short full-scale L-shaped prestressed spandrel beams so as to determine if it would be probable to do away with closed stirrups. The samples included different transverse and longitudinal reinforcement conformations, but closed stirrups were purposely left out. The results exhibited that although longer beams displayed skewed-diagonal and wide diagonal cracking as a result of the combined effects of shear and torsion, shorter beams mainly encountered local ledge failures. The failure pattern was displayed to change with the additional longitudinal reinforcement in flexural, indicating the crucial role that reinforcement details play in resistance to complicated stress states.

Hassan et al. (2007) [6] conducted a nonlinear finite element study investigating the shear response of prestressed L-shaped spandrel beams, with the attention on punching shear of the spandrel ledge, a critical failure mode. The PCI design parameters significantly overvalued the punching shear capacity by about 50–60%, according to a comparison of the numerical data with the provisions. Furthermore, parametric testing showed that while increasing the prestressing level greatly increased punching shear strength, resulting in gains of up to 40%, increasing concrete compressive strength only enhanced its strength by roughly 13%.

Using ABAQUS/Standard, Mercan et al. (2010) [7] developed a finite element model of precast, prestressed concrete spandrel beams. Reliability was guaranteed by validating the numerical results with the existing experimental data. Finite element type, fracture energy, concrete dilation angle, bearing stress distribution, tension stiffening, and support conditions were among the material parameters and modeling assumptions that their study looked at. The analysis exhibited that the choice of finite element type, the assumed concrete dilation angle, the stiffness of the deck-to-spandrel connections, and the distribution of bearing stresses at the supports all have a significant influence on the structural response of precast, prestressed spandrels under vertical loading.

Salman & Ali (2015) [8] conducted a numerical analysis on the strength and response of hollow and solid spandrel beams under impact loading and compared their predictions with similar experimental data obtained from the literature. They studied how the global response of the beams was influenced by flanged floor beam sections with different depths

and flange widths. In terms of the ultimate load, angle of twist, and ultimate torque, the results exhibited a significant level of agreement between the numerical results and experimental benchmarks. Additionally, it was found that flange depth and width had a significant effect on structural performance: samples with larger flange widths exhibited roughly 21.44% greater ultimate load capacity compared to narrower sections, and flanged sections obtained up to 156% higher torque transfer than rectangular sections.

Hussein et al. (2017) [9] studied an experimental, numerical, and theoretical investigation on the effect of internal vertical stirrups on the hanging action of ledge beams. ABAQUS was used to simulate and evaluate four simply supported L-shaped beams with different internal stirrup configurations under mid-span loading. When compared to a beam with only external stirrups, the results exhibited that the presence of internal stirrups significantly increased hanger load capacity, with increases of 17%, 8%, and 3% for stirrup spacings of 40 mm, 70 mm, and 100 mm, respectively. These results were generally in line with the PCI manual [10], while a few differences were noted with regard to the PCA notes on ACI 318-14 [11]. Numerical and experimental results were in good accord with analytical predictions.

Hariharan et al. (2019) [12] experimented with the full-size L-beams to confirm the possibility of the application of open web reinforcement instead of closed stirrup reinforcement. The outcome indicated that the open web reinforcement plus segmented reinforcement is a good choice of L-beams, whereas the reference beam of closed stirrups produced greater end-region resistance. The research suggested inverted U-shaped or C-shaped forms to improve structural performance in general and the reinforcement of the top web to prevent shallow-angle cracking and increase control of the cracks.

In recent years, fiber-reinforced polymer (FRP) composites have gained more popularity in civil engineering because of their proven capability to increase the impact resistance of structural buildings. They have been commonly used in many different applications to retrofit and strengthen both new and old elements, such as walls, slabs, bridges, and columns [13].

Salom et al. (2004) [14, 15] examined the experimental and analytical research on the reinforced concrete spandrel beams; this research investigates the torsional strengthening using carbon fiber-reinforced polymer (CFRP) laminates. For separation and evaluation of the contribution of the carbon fiber polymer-reinforced (CFRP) system to torsional strength, the specimens were subjected to pure torsional stress. Important variables such as fiber orientation, lamination type, and the presence of a fixing mechanism were investigated. The experimental results verified that the use of CFRP significantly enhanced torsional resistance, reaching increases of up to 77%. The main causes of the beam failure were extensive concrete cracking, followed by separation of the composite lamination layers. In addition, an analytical model on the basis of popular torsional strength concepts and shear retrofit equations has been presented, which proved to be in good correspondence with the experimental results and proved the efficiency of the strengthening method. Other current studies have concentrated on strengthening and repairing reinforced concrete (RC) beams subjected to torsional loads with methods including strip-wrapped ferrocement, continuous spiral near-surface installed steel wire ropes, and externally bonded CFRP sheets [16-19].

Ayaad & Oukaili (2023) [20-22] examined the effect and torsional performance of 6 L-shaped reinforced concrete (RC) spandrel beams under eccentric impact loading, highlighting the effectiveness of different types of strengthening. Two techniques were investigated, which are embedded through-section (ETS) steel bars and externally bonded carbon fiber-reinforced polymer (CFRP) sheets. The research findings indicated that ETS bars enhanced torsional strength and residual static strength by up to 27.5%, and CFRP sheets enhanced impact strength by up to 46%. The findings also demonstrated that high-impact loads are a result of high stiffness.

Kawarai et al. (2025) [23] experimentally investigated the low-velocity impact-load-carrying behavior of RC beams strengthened in flexure by bonding CFRP sheets to the tension-side surface. Drop-weight impact tests using a 300 kg steel weight were conducted on beams strengthened with different CFRP sheet areal masses. The results showed that the amount of CFRP affected the impact resistance and failure mode, where sheet rupture or intermediate-crack debonding controlled the ultimate response. This study confirms that CFRP sheets can enhance the impact resistance of RC beams, but debonding and rupture mechanisms must be carefully considered.

Saad et al. (2025) [24] numerically studied full-scale RC beams with web openings subjected to low-velocity impact loading and investigated the effectiveness of externally bonded CFRP strengthening. The study examined the influence of opening location, opening dimensions, and CFRP reinforcement on impact behavior. The results indicated that larger shear-zone openings benefited significantly from CFRP strengthening, while CFRP application reduced peak deflections and improved load transfer around the openings. Their findings support the use of CFRP sheets to mitigate impact-induced damage and improve the dynamic performance of deficient RC beams.

Homayoonifar et al. (2026) [25] experimentally examined RC panels strengthened with different CFRP sheet patterns under repeated drop-weight impact loading. Eight panels were tested, including control specimens and panels strengthened using different CFRP layouts. The results showed that CFRP strengthening generally improved impact resistance, increased absorbed energy, delayed severe damage, and helped control cracking and fragmentation. The most

effective layout, with two CFRP sheets applied in the mid-strip regions on the tension face, sustained 160 impacts until perforation and achieved a 63% increase compared with the control specimens.

Duan et al. (2025) [26] conducted an experimental investigation to study the mode of failure and crack development of CFRP-strengthened concrete beams subjected to both static and impact loads. Varied lengths of CFRP cladding were applied to each beam in order to conduct an analysis of the results through the use of digital image correlation (DIC) for measurements of both crack propagation and evolution of damage. The analysis of the results showed that there was a significant change in the way that crack was developed based on the configuration of the CFRP, e.g., significantly affecting impact resistance and the development of mode failure. As a result, it can be concluded that the efficiency of CFRP-strengthened concrete beams under impact loads is a function of not only the presence of the CFRP sheets but also the lengths of strengthening, bond conditions, and the interaction between the CFRP layer and the concrete substrate.

Luo et al. (2026) [27] studied the impact and post-impact performance of strengthening RC beams with near-surface mounted (NSM) CFRP strips through tests of impact loading, post-impact static loading tests, and numerical simulations by the LS-DYNA program. The main variables for this study included strengthening technique and comparison between unstrengthened beams, externally sheet-bonded CFRP-strengthened beams, and NSM CFRP-strengthened beams. Their results exhibited that NSM CFRP strengthening enhanced the dynamic response, residual capacity of load-carrying, energy dissipation, and post-impact performance of the beams compared with conventional externally bonded strengthening.

A careful synthesis of the reviewed literature reveals a temporal gap in the reviewed literature on precast L-shaped spandrel beams. Decades after the few field results from early investigations in the 1960s [28, 29], more structured testing in the 1980s focused on the effects of eccentric loading (e.g., Klein (1986) [30]). The 2000s saw a resurgence of research (e.g., Lucier et al. (2007-2011) [5, 31, 32]), with a focus on open web reinforcement setups and the creation of rational design approaches. However, there is a noticeable discontinuity in the advancement and continuity of research on spandrel beam behavior, as evidenced by the length of time between these efforts, most notably in the 1960s and 1980s and again between 1986 and 2011.

From a thematic standpoint, almost all previous study has focused on assessing reinforcement detailing techniques (e.g., closed-web stirrups versus open-web reinforcement) and torsional and shear behavior under static or single-impact loading. The nonlinear interaction between inertia forces and reaction forces, the strengthening of spandrel beams with CFRP under such loading, and repeated impact loads have all not been studied. Understanding the dynamic behavior of these structurally important parts is severely hampered by this omission. Specifically, how the reaction forces from progressive damage, inertia force evolution, midspan deflection varying, residual behavior, and damage accumulation progress through multiple impacts have only been reported very minimally in the available literature. This limitation is partially due to the difficulty of obtaining complete force histories and damage reports associated with repeated drop-weight impact testing.

Therefore, by specifically examining L-shaped spandrel beams exposed to repeated impact events both before and after CFRP strengthening, the current study offers a novel contribution. By doing this, the study tackles the theme shortcomings and chronological discontinuities seen in the body of current literature.

Finite element analysis (FEA) is still an effective technique for gaining a deeper understanding of the complex response of compact and slender L-shaped spandrel beams, even though several research have used finite element simulations. The current study numerically investigates the impact and torsional behavior of L-shaped RC spandrel beams reinforced with CFRP sheets in order to fill in the remaining knowledge gaps. It focuses on how these beams respond to repeated vertical impact loading. To ensure the accuracy as well as reliability of the numerical predictions, a comprehensive finite element model was created in ABAQUS and verified against the experimental program carried out by Ayaad & Oukaili [20, 22]. The chosen architecture allows for a targeted and measurable evaluation of the performance gains brought about by CFRP strengthening, even though further case studies could increase generality.

The numerical approach of this study is to extend the interpretation of the previous experimental work by quantifying the repeated-impact degradation of reaction force and the evolution of inertia force, which were not fully detailed in the original test program. The study also assesses the effectiveness of CFRP strengthening in improving stiffness retention, making inertia force response more controlled, reducing deflection, enhancing residual performance, and limiting progressive damage. The structure of this paper is as follows: The experimental program used for model validation is described in Section 2, the finite element modeling procedure is presented in Section 3, the numerical results, including force partitioning and damage evolution, are discussed in Section 4, and the study's main conclusions and contributions are summarized in Section 5. The overall numerical workflow adopted in this study is summarized in Figure 2.

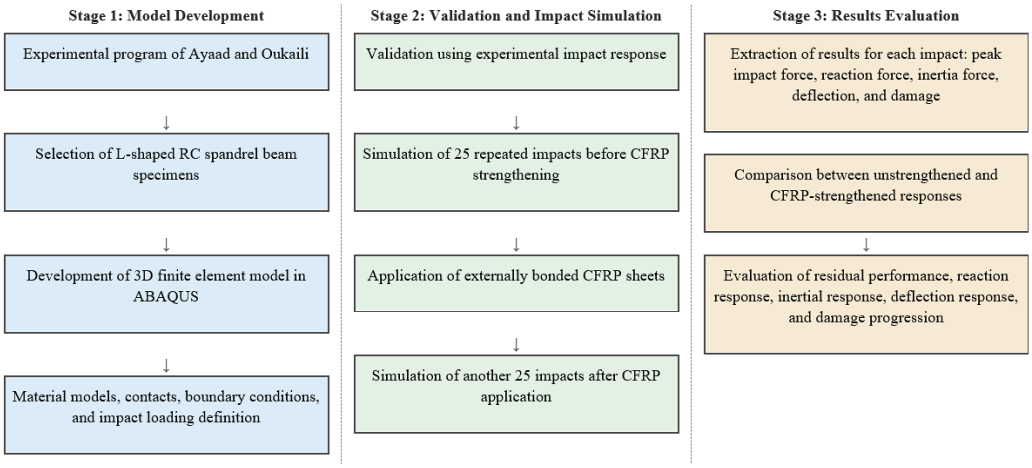

Stage 1 → Stage 2 → Stage 3

Figure 2. Flowchart of the numerical methodology adopted in this study

2. Experimental Work

Ayaad & Oukaili carried out experimental research on the impact resistance of reinforced concrete ledge beams [20–22]. Four L-shaped spandrel specimens with an overall length of 1500 mm and an effective span of 1300 mm were developed and tested as simply supported beams. Each specimen had a ledge that measured 250 × 200 mm, with two beams having a web cross-section of 650 × 150 mm and the other two having a web cross-section of 450 × 150 mm. The equivalent web slenderness ratios h_w/b_w where b_w denotes the web thickness; were roughly 4.33 and 3.00, respectively. These values show that while the second pair of beams is at the lower end of slender behavior, the first pair has a clearly slender web [33]. The geometric features of these specimens directly affect their shear, torsional, and impact responses because slender webs are more prone to lateral instability, decreased torsional stiffness, and stress concentration at the web–ledge junction.

In order to recreate the optimal configuration, anchor the web to the testing rig's rear supporting columns, and permit unrestrained torsional deformation, the original ledge was trimmed by 150 mm at each end, resulting in a total ledge length of 1200 mm.

A 26.5 kg steel mass dropped from a height of 1.0 m onto the ledge at mid-span was used to subject the beams to vertical impact loading. The impact point was placed 150 mm away from the web's front face. The associated impact velocity (v) was calculate using the free-fall formula $\sqrt{2gh}$, where h is the drop height and g is the gravitational acceleration, providing the initial kinetic input for assessing the beams" dynamic response. Steel bearing plates measuring 100 × 150 mm were used to offer support conditions. They were centrally aligned with the web to guarantee appropriate vertical load transfer. During testing, the web was restrained at both ends to preserve lateral stability. Four transverse holes, two at each end, were drilled through the web to accept high-strength threaded bars in order to fasten the beams to the testing rig.

The PCA Notes on ACI 318 11 [34] and the guidelines of ACI 318 19 [35], which directed the reinforcement detailing, were followed in the design of the four specimens. Every beam was set up to withstand combined shear-torsion and torsion stresses. More flexural and ledge reinforcement was added to ensure that the load from the drop mass was efficiently distributed to the web and to lower the possibility of local ledge collapse during impact. Figure 3 displays the specimens' overall geometry and cross-sectional measurements.

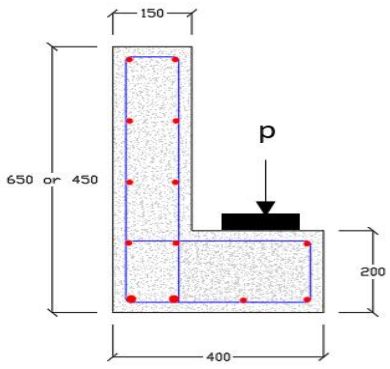

Figure 3. Cross section and dimensions of reference and strengthened specimens (all dimensions are in mm)

Each spandrel beam included deformed steel reinforcement to resist the combined forces of torsion, shear, and bending. The outside legs of the closed web stirrups serve as ledge hangers and bear torsional stresses in accordance with applicable code regulations. The beams' ability to resist bending, torsion, and shear-torsion demands under applied loads is guaranteed by this specification. Every specimen used the same arrangement of reinforcement. In both the web and the ledge, longitudinal torsional bars were placed along the inside perimeter of the closed stirrups, with a minimum of one bar anchored at each corner.

Additional longitudinal reinforcement was provided in the bottom tension zone of the web to satisfy flexural requirements, while 10 mm closed stirrups spaced at 250 mm, together with longitudinal bars of the same diameter, resisted shear–torsion stresses. Two 16 mm tensile bars formed the primary flexural reinforcement at the soffit, and the ledge was detailed with 12 mm closed stirrups spaced at 60 mm to prevent punching shear and to transfer loads from the ledge to the web. The reinforcement layout is illustrated in Figure 4.

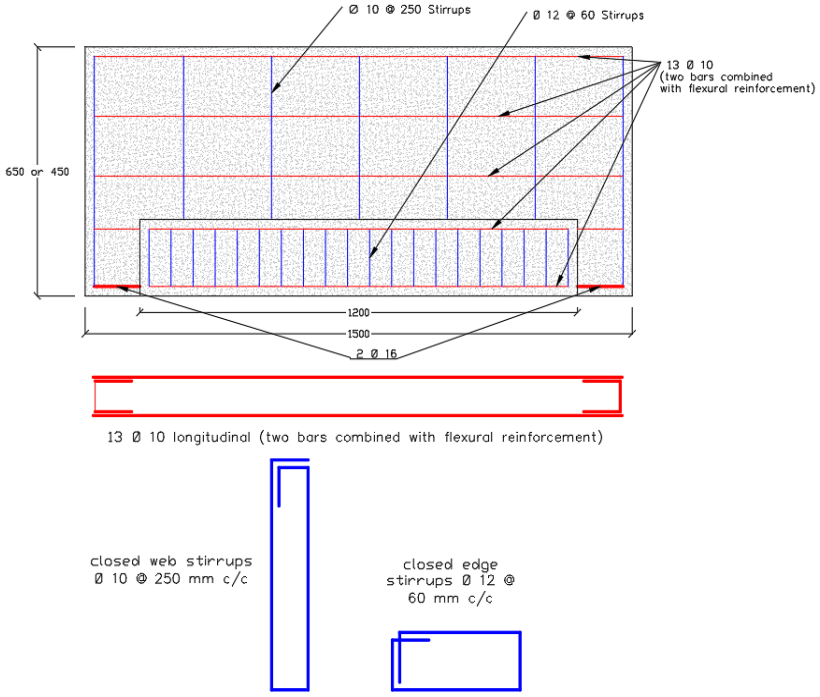

Figure 4. Reinforcement details of tested specimens (all dimensions are in mm)

The experimental program included two reference specimens: SB1-US-D, a slender beam with an aspect ratio of 4.33, and SB2-US-D, a moderately slender beam with an aspect ratio of 3.0. Two corresponding strengthened specimens, SB1-CS-D and SB2-CS-D, were reinforced with CFRP strips while maintaining the same aspect ratios as their respective reference beams.

The arrangement of the specimen notation is as follows: A spandrel beam is denoted by SB. The number 1 denotes an aspect ratio of 4.33, which is categorized as a slender beam, while the number 2 denotes an aspect ratio of 3.0, which is the lowest limit of slender behavior for the chosen geometry. Unstrengthened and CFRP-strengthened specimens are denoted by the labels US and CS, respectively. The specimen was tested under impact loading, as indicated by the final letter D.

In order to distinguish between unstrengthened and strengthened specimens, the impact testing methodology included two loading phases. Each specimen was tested for 25 impact events for the unstrengthened beams, which were created by dropping a 26.5-kg load onto the ledge from a height of 1.0 m. Two stages of testing were carried out for the reinforced beams. Initially, 25 impact events were applied to each specimen in an identical technique to its unstrengthened counterpart. After adding carbon fiber reinforced polymer (CFRP) strips for external strength, the beam was subjected to 25 more impact events with the same drop height and loading configuration. The strengthening system was made up of 150-mm-wide CFRP strips that were evenly spaced at 60 mm intervals and fully wrapped the cross-section's perimeter. The CFRP and the concrete surface were properly bonded due to a structural epoxy adhesive.

3. Finite Element Model Description

Finite element (FE) simulations of RC spandrel beams, in both unstrengthened and CFRP-strengthened conditions, were performed using ABAQUS [36] in accordance with the ABAQUS User's Guide [37]. The analyses employed the ABAQUS/Explicit solver to capture the nonlinear transient response under impact loading. Material properties assigned

to concrete, steel reinforcement (with the specified bar diameters), and CFRP are reported in Table 1 and were implemented through constitutive descriptions that represent concrete cracking and crushing, steel yielding, and the interaction between reinforcement and concrete. The numerical model was verified by comparison with experimental data available in the literature [22], indicating that the model has the ability to reproduce both global and local structural responses.

Table 1. Properties of materials

Concrete				
Specimen IDs	SB1-US-D	SB1-CS-D	SB2-US-D	SB2-CS-D
Cylinder compressive strength f_c' (MPa)	45.46	46.20	44.70	45.13
Tensile strength f_{ct} (MPa)	3.85	4.10	3.68	3.82
Modulus of elasticity E_c (MPa)	32060	32216	31570	32150
Steel Bars				
Diameter (mm)	10	12	16	
Yield strength f_y (MPa)	575.00	605.05	612.67	
Tensile strength f_u (MPa)	670.67	698.00	707.00	
Elongation (%)	9.34	9.42	11.18	
GFRP Sheets				
Tensile strength f_{fu} (MPa)	4100			
Modulus of elasticity E_f (MPa)	230000			
Elongation (%)	1.7			

The geometric and material modeling parameters were carefully selected to simulation the behavior of the tested specimens as accurately as possible, which was necessary to obtain accurate results for the response of RC spandrel beams under repeated loading. Each beam was experimented on with a repeated-impact protocol with 25 events of impact loading during the unstrengthened stage and 25 other events of impact loading after strengthening stage with CFRP (50 events in total). The given procedure allowed a close evaluation of the progressive structural response, with special consideration to the changes in impact and reaction forces during the process of damage. In the present study, the theoretical approach was expressed to investigate the relationship between impact force, reaction force, inertia force, and number of repeated impacts. The concept of the analysis was based on the fact that repeated impact loading produces cumulative damage in the RC beam; thus, each following impact does not act on an intact specimen but on a specimen with reduced stiffness, accumulated cracking, residual deformation, and redistributed stresses from the prior impact. Accordingly, the procedure of numerical modeling was designed to preserve the damage after each impact event and use it as the initial condition for the following impact event. Thus, the theoretical–numerical approach of the present study was not limited to reproducing the experimental results but also aimed to evaluate the progressive variation of reaction force and inertia force with the number of impacts, as well as cases that were not fully informed in the experimental study.

3.1. Model Components and Element Types

This subsection will identify the finite element model's part and element types assigned to them in the model. The selected elements will allow for correct transfer of stress in the model, accurate explicit analyses, and appropriate modelling of the dynamic response of the structures as observed in the laboratory. Concrete components such as spandrel beams, bolts, load plates, lateral plates and support plates were modeled as solid brick elements having 8 nodes (C3D8R). In the explicit simulations, single point reduced integration was used to prevent hourglassing and provide numerical stability.

In order to simulate the reinforcing steel, such as longitudinal bars and stirrups, it was represented as one-dimensional deformable members (wire type) with three-dimensional, two-node linear trusses (T3D2). Each element possesses three degrees of translation (Ux, Uy, and Uz), which enables complete modeling of axial deformation and load transfer within the reinforced concrete system.

To accurately simulate the twisting, bending, and in-plane performance, the four-node shell elements (S4R) were used to represent the sheets of the CFRP applied to the strengthened beams, and each node had six degrees of freedom: three translational and three rotational. In these factors, ABAQUS/Explicit employs hourglass control, linear interpolation, and reduced integration to offer numerical integrity and to prevent undue deformations in the time course of the dynamic impact simulations.

Boundary conditions were accurately simulated by using realistic support conditions and modeling the impactor as a discrete rigid element (R3D4). The use of rigid elements confirms an effective and reliable study of the beam's reaction under impact loading by simplifying the representation and reducing the simulation's processing effort.

3.2. Constitutive Material Properties

Reliable simulation of reinforced concrete spandrel beams under impact loads needs accurate material behavior modeling. In order to accurately represent their nonlinear behavior, this subsection defines the constitutive models and important attributes assigned to concrete, steel reinforcement, bolts, plates, and CFRP sheets in the finite element model.

Concrete was simulated using the Concrete Damage Plasticity (CDP) model [38, 39] as implemented in ABAQUS [37], this model was selected because it is capable of representing the main nonlinear damage mechanisms of concrete, including tensile cracking, compressive crushing, stiffness degradation, and damage accumulation. According to the ABAQUS documentation, the CDP model is a continuum plasticity-based damage model for concrete, in which the main failure mechanisms are tensile cracking and compressive crushing. In addition, previous impact-related numerical studies have used the CDP model for reinforced concrete structures subjected to impact loading and have investigated the sensitivity of the response to CDP parameters and mesh size [40]. The adopted parameters were a dilation angle (ψ) of 36°, flow eccentricity (ε) of 0.1, a biaxial-to-uniaxial compressive strength ratio (f_{bo}/f_{co}) of 1.16, a shape factor (k) of 0.667, and a viscosity parameter (μ) of 1×10^{-4}. These values were selected in accordance with ABAQUS guidelines, calibration studies, and literature recommendations, all of which generally state that they provide realistic behavior and reliable convergence in dynamic and impact simulations [41–44]. Tensile cracking and compressive crushing are the two main mechanisms of failure involved in the isotropic CDP model (see Figure 5) [36]. Hordijk's simplified tension-softening model [45], which offers a realistic.

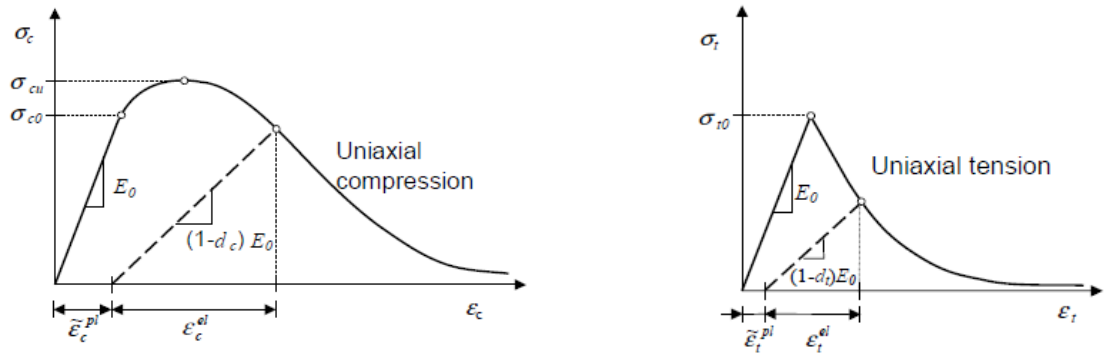

Figure 5. Behavior of concrete (a) Uniaxial Compression and (b) Uniaxial tension (Abaqus User Manual [37])

depiction of fracture initiation and post-peak softening, was used to determine the concrete stress-strain response under uniaxial tension. The Saenz basic law [46], which accounts for both the descending post-peak crushing response and the ascending nonlinear branch, was used to simulate the nonlinear concrete behavior under uniaxial compression.

For the reinforcing steel, the Johnson–Cook plasticity model was adopted to account for the strain-rate-dependent plastic behavior induced by impact loading. The Johnson–Cook model was originally proposed for metals subjected to large strains, high strain rates, and high temperatures [47]. Furthermore, the ABAQUS documentation states that the Johnson–Cook model is suitable for high-strain-rate deformation of metals in dynamic simulations [48]. Since repeated impact loading can generate high strain-rate effects in the reinforcement, the Johnson–Cook model was considered more appropriate. In contrast, the bolts and plates, also made of steel, were modeled as linearly elastic isotropic materials, with a Poisson's ratio of 0.3 and a modulus of elasticity of 200,000 MPa, representing their linear elastic behavior under the applied loads.

In ABAQUS/Explicit, a damage model is available that predicts the initiation of damage and captures damage evolution for elastic-brittle materials with orthotropic behavior, making it suitable for modeling CFRP [37, 49]. The modeling of CFRP is conducted in three stages: first, the material is assigned a linear elastic response; second, a damage initiation criterion is applied to define the onset of failure; and third, a damage evolution law governs the progressive degradation of the composite.

3.3. Element Contact Modeling

Element contact and interaction are essential in all types of FE. ABAQUS provides various contact interaction models, each representing surface behavior. In this study, the connection between steel reinforcement and surrounding concrete was simulated using an embedded method, ensuring full composite action. To prevent relative

motion between surfaces, tie constraints were applied: between the steel load plate and the concrete surface, and between the CFRP sheets and the concrete, reflecting the experimental observation that no CFRP debonding occurred [20, 22], see (Figure 6, right). The impact load interaction with the top surface of the beam was modeled using surface-to-surface contact in ABAQUS/Explicit, employing a penalty-based contact formulation with small-sliding assumptions (Figure 6, left). This arrangement permits relative sliding at the contact interface while guaranteeing correct load transmission simulation.

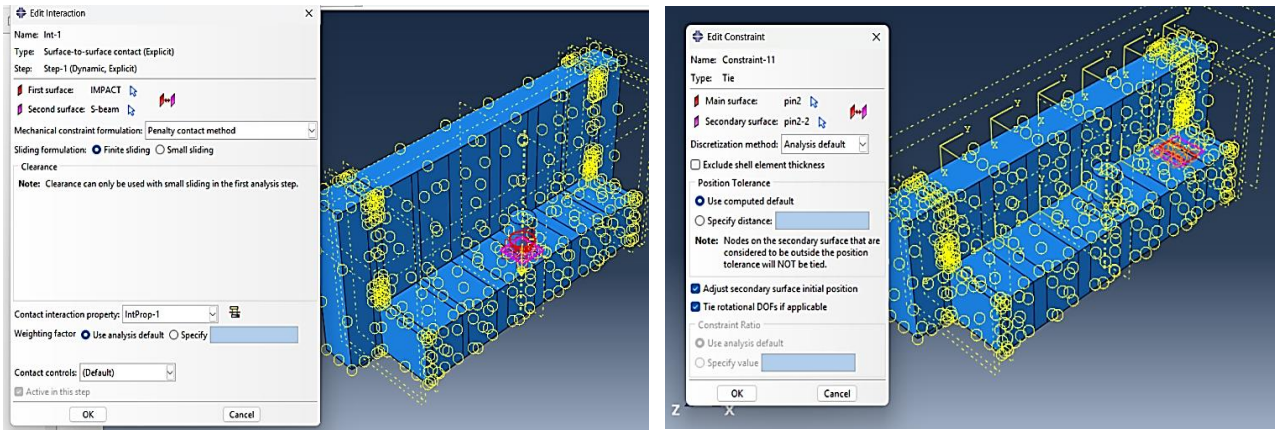

Figure 6. Definition of contact (left) and tie (right) interactions used in the simulation

3.4. Boundary Conditions and Impact Load Application

For defining loads, boundary conditions, and initial conditions in a finite element model, Abaqus provides several methods. Each boundary, load, or initial condition must be allocated to the particular analysis step in which it becomes active because these definitions are step-dependent.

In accordance with the experimental setup, the specimens were tested under simply supported conditions. To accurately reproduce this in the FEM, one end of the beam was modeled as a pinned support, while the opposite end was represented as a roller support. The pinned support was constrained against displacement in both the longitudinal and vertical directions, whereas the roller support was restrained only in the vertical direction (Figure 7).

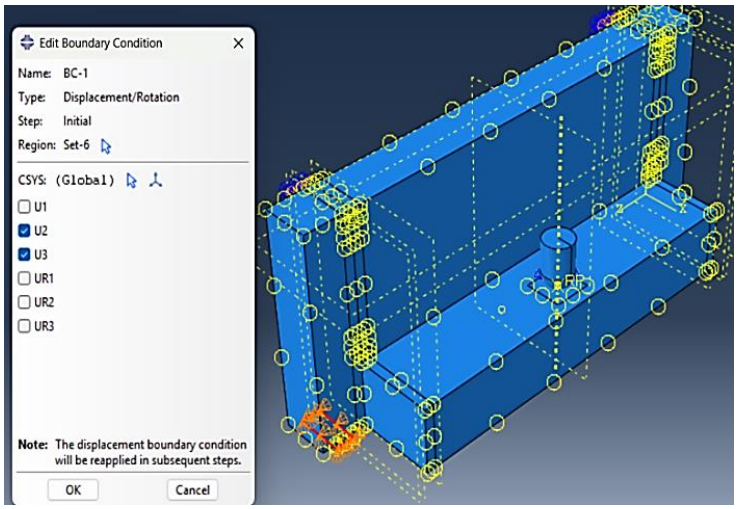

Figure 7. Boundary conditions applied to the simply supported spandrel beam in the finite element model

An additional boundary condition was applied to ensure that the impactor moved strictly in the vertical direction. For this purpose, a geometry set corresponding to the upper circular surface of the impactor was defined, and a displacement/rotation boundary condition was assigned to regulate its degrees of freedom. A predefined translational velocity was applied to the impactor's upper surface in the Y-direction to enforce strictly vertical motion, while all other translational and rotational degrees of freedom were fully restrained. All boundary conditions for the supports and the impactor were introduced during the initial step of the analysis.

The initial velocity of the projectile (drop weight) was simulated by assigning each node a velocity calculated as $v = \sqrt{2gh}$ oriented perpendicular to the ledge of the spandrel beam surface. This velocity was implemented in the model as a predefined field (Figure 8).

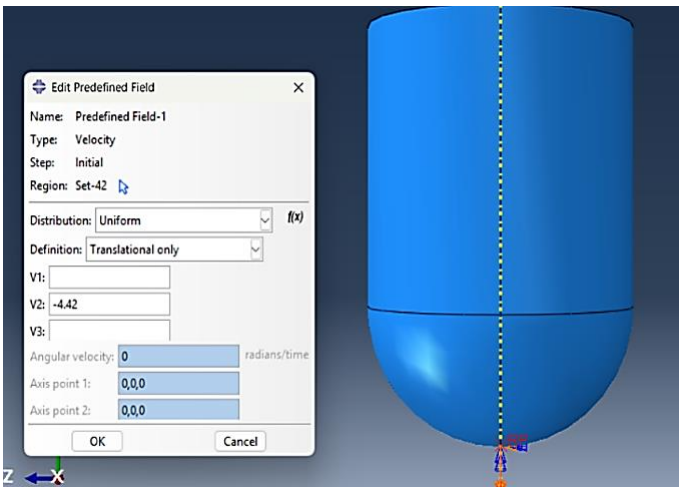

Figure 8. Definition of the initial velocity field for the drop-weight impact in the simulation

To obtain the structural response, the simulation used an explicit dynamic step in ABAQUS. The repeated low-velocity impacts were modeled as a series of individual impacts. When the specified time interval of the initial impact step was reached, the simulation ended and all the results were recorded to the Output Database (ODB) file for post-processing. For subsequent impacts, effects, structural state variables of plastic strains and stress fields were transferred between the impact before and after by the predefined initial state approach. There were re-applications of the same boundary and loading conditions to every cycle so that realistic repetition of the impact behavior could be simulated. The cumulative damage approach using initial state transfer was selected because it allows the accurate transfer of stress and strain fields between successive impacts, ensuring the accumulation of damage is correctly represented. Alternative strategies, such as restart simulations or continuous simulations, could also be used; however, restart simulations require multiple independent runs and increased user intervention, while fully continuous simulation can become computationally expensive and difficult to control when a large number of impacts is considered. Therefore, the initial state transfer method was adopted as a practical and efficient approach for representing cumulative damage under repeated impact loading.

3.5. Finite Element Mesh

The three-dimensional model had a 2-node linear truss element (T3D2) as its model of reinforcing bars, and an 8-node linear brick element with a smaller integration (C3D8R, Figure 9) as its model of concrete. The CFRP layer was modeled by using four-node quadrilateral shell elements (S4R), and the steel projectile was modeled as a rigid body by using four-node quadrilateral shell elements (R3D4). The hourglass control and distortion control were adopted in an attempt to avoid the problem of numerical instabilities and excessive element deformation.

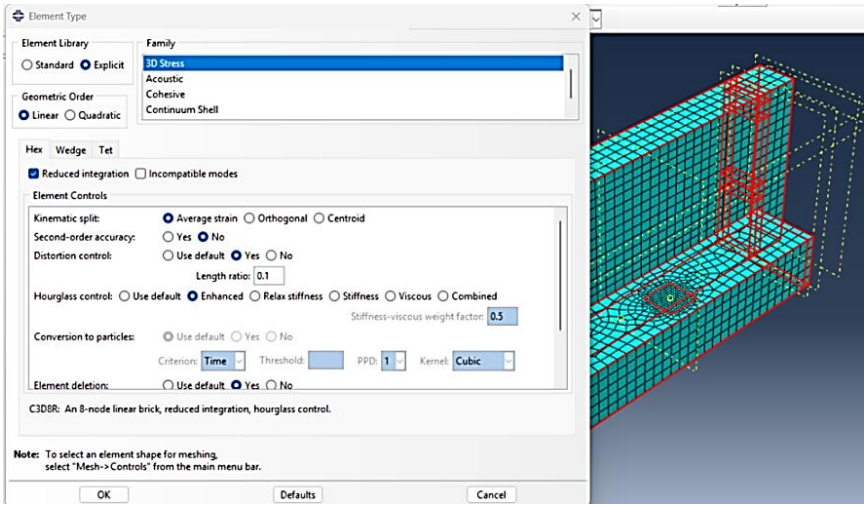

Figure 9. Definition of C3D8R elements with distortion and hourglass control parameters

A finer mesh was adopted in critical regions, such as the impact zone and near supports, to ensure solution accuracy, whereas a coarser mesh was used in less critical regions to reduce computational cost. A mesh convergence study confirmed that further refinement did not significantly affect the results.

4. Results and Discussion

The experimental dataset used to validate the numerical model was obtained from the study by Ayaad & Oukaili [20, 22]. To maintain consistency with the original experimental program, both the strengthened specimens (SB1-CS-D and SB2-CS-D) and the reference specimens (SB1-US-D and SB2-US-D) were modeled and analyzed. The impact force–time, reaction force-time, and displacement–time histories for all specimens, obtained from both experimental and numerical analyses, are presented in Tables 2 to 4 and illustrated in Figures 10 and 11.

Table 2. Midspan deflection; experimental and numerical data

Specimens ID	Midspan Deflection, (mm)											
	Stage-1 (before strengthening)						Stage-2 (after strengthening)					
	Experimental data		Numerical data		Difference%		Experimental data		Numerical data		Difference%	
	Event-1	Event-25	Event-1	Event-25	Event-1	Event-25	Event-1	Event-25	Event-1	Event-25	Event-1	Event-25
SB1-US-D	1.35	2.54	1.22	2.65	-9.6	+4.3						
SB1-CS-D	1.33	2.50	1.20	2.6	-9.8	+4.0	1.25	2.0	1.10	2.10	-12.0	+5.0
SB2-US-D	1.50	2.83	1.40	3.0	-6.7	+6.0						
SB2-CS-D	1.52	3.00	1.41	2.8	-7.2	-6.7	1.40	2.31	1.25	2.15	-10.7	-6.9

Table 3. Impact force; experimental and numerical data

Specimens ID	Impact Force, (kN)											
	Stage-1 (before strengthening)						Stage-2 (after strengthening)					
	Experimental data		Numerical data		Difference%		Experimental data		Numerical data		Difference%	
	Event-1	Event-25	Event-1	Event-25	Event-1	Event-25	Event-1	Event-25	Event-1	Event-25	Event-1	Event-25
SB1-US-D	70.54	53.75	81.00	44.20	+14.80	-17.80						
SB1-CS-D	71.20	53.57	83.00	49.90	+16.60	-6.90	92.56	78.14	102.00	71.50	+10.20	-8.50
SB2-US-D	73.20	54.76	81.00	44.00	+10.70	-19.60						
SB2-CS-D	72.53	54.59	81.50	45.80	+12.40	-16.10	93.56	79.72	101.10	69.00	+8.10	-13.40

Table 4. Reaction force; experimental and numerical data

Specimens ID	Reaction Force (kN)									
	Stage-1 (before strengthening)						Stage-2 (after strengthening)			
	Experimental data		Numerical data		Difference%		Experimental data		Numerical data	
	Event-1	Event-25	Event-1	Event-25	Event-1	Event-25	Event-1	Event-25	Event-1	Event-25
SB1-US-D	52.76	39.77	79.70	36.10	+51.10	-9.20				
SB1-CS-D	53.40	40.45	82.00	38.00	+53.60	-6.10	N/A	N/A	97.50	61.50
SB2-US-D	54.90	41.80	77.80	33.20	+41.70	-20.60				
SB2-CS-D	54.25	39.85	78.00	32.00	+43.80	-19.70	N/A	N/A	96.30	58.70

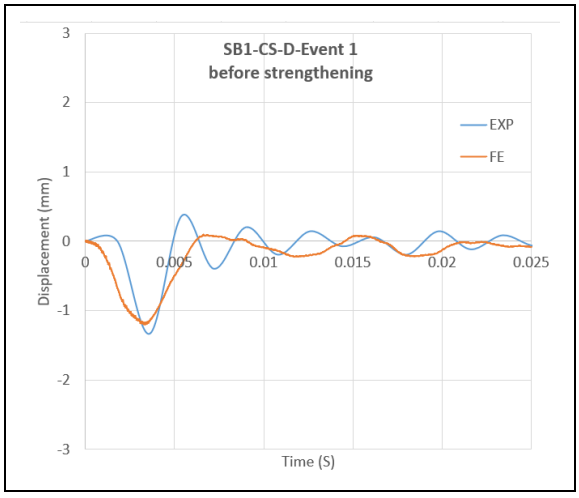

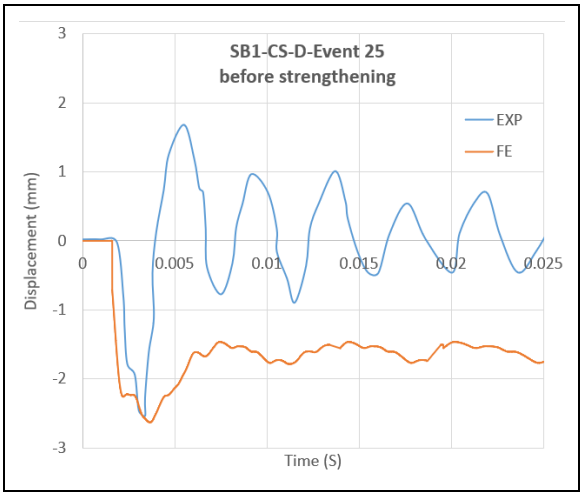

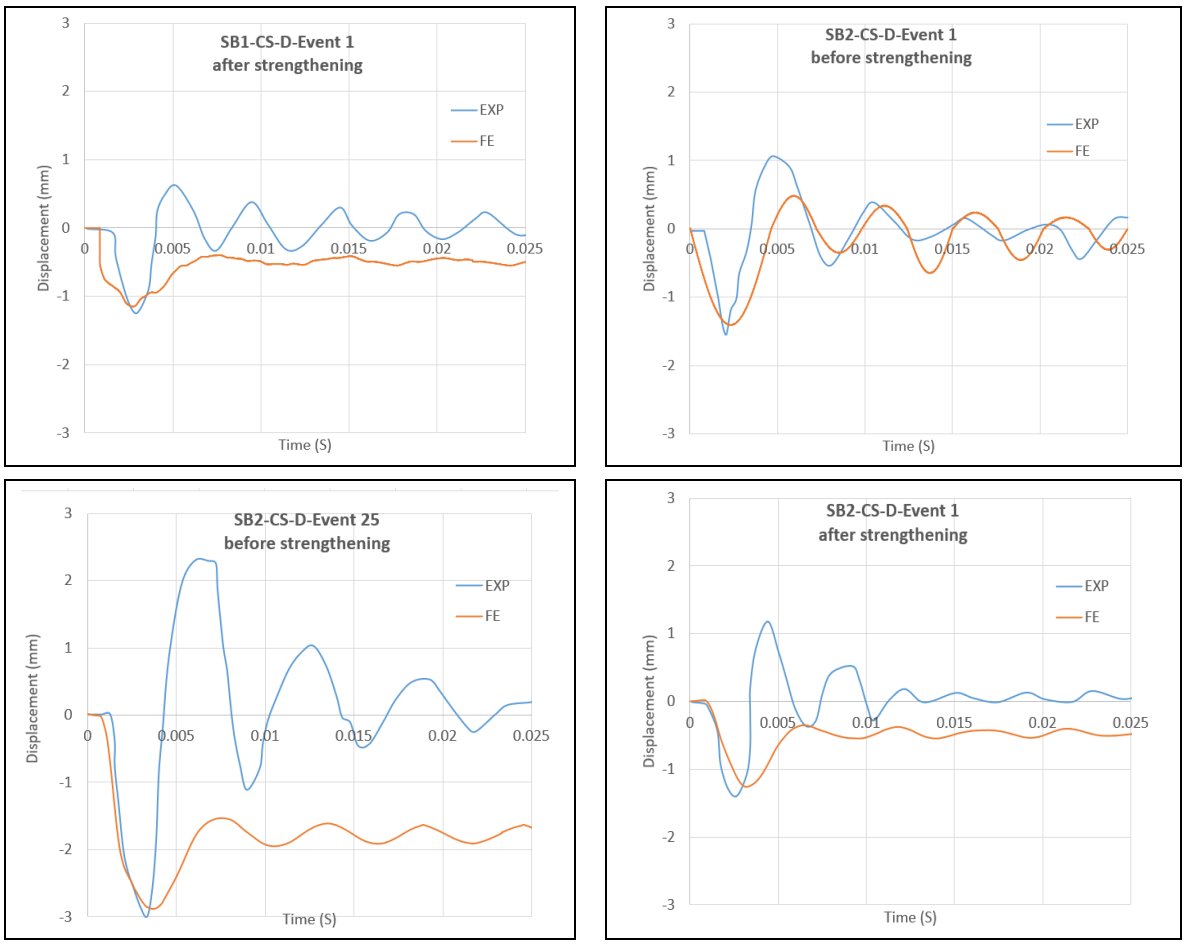

Figure 10. Time-history displacement comparison for tested ledged beams: experimental vs. FE

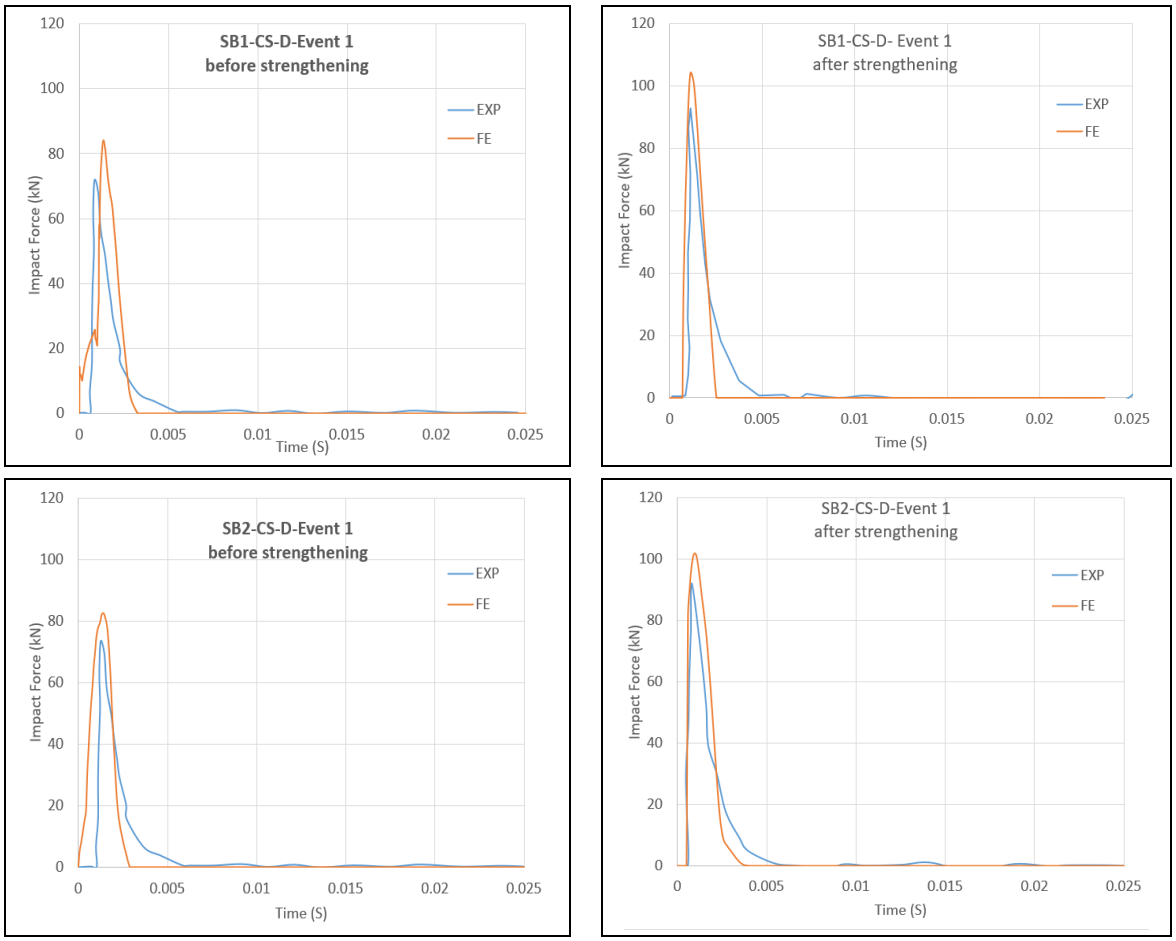

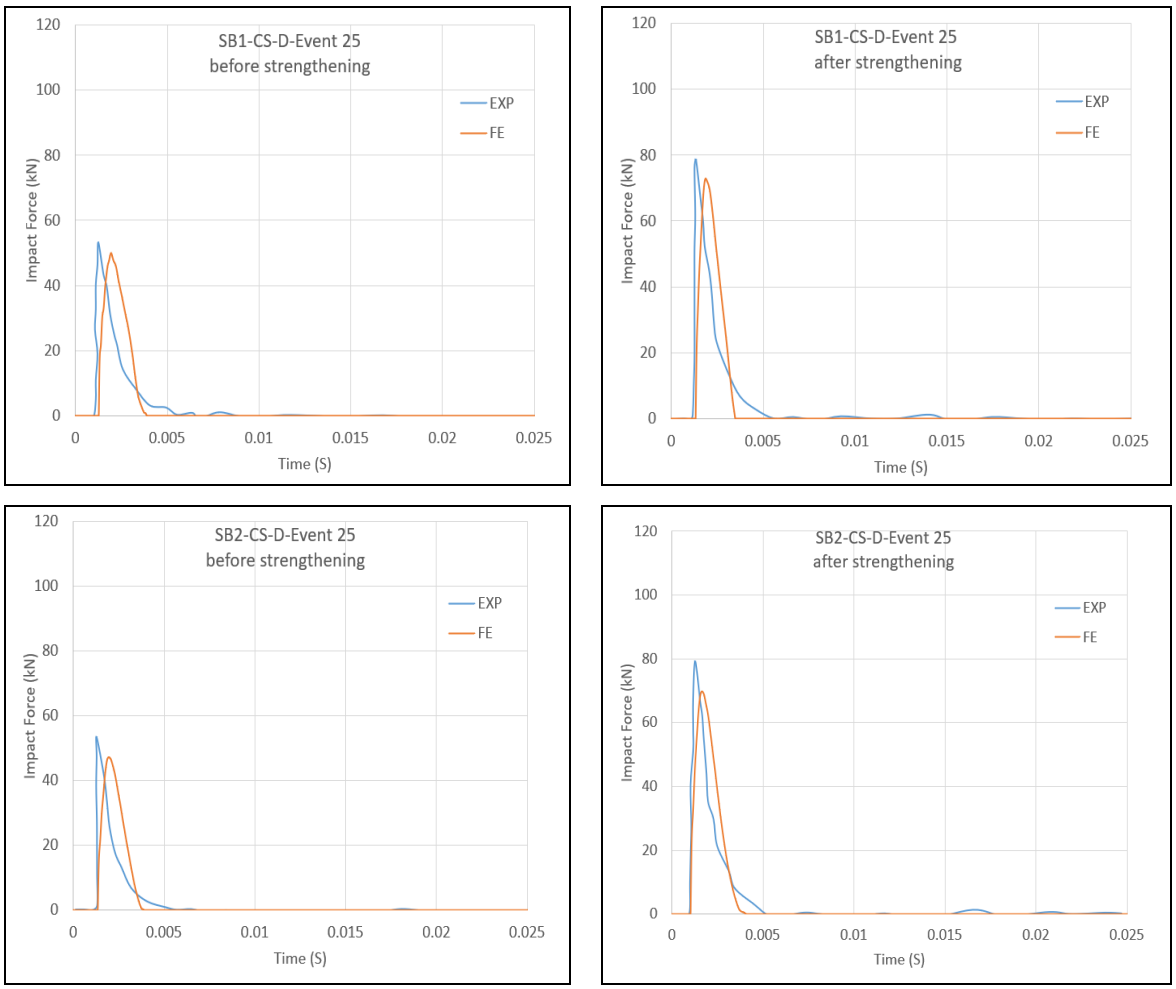

Figure 11. Time-history of impact force for tested ledged beams: experimental vs. FE

Since the compressive strength of the concrete in the reference beams differed only slightly (by approximately 1 MPa) from that of their strengthened counterparts, the impact force, reaction force and deflection results were in close agreement between the two groups, showing only minor differences. The reference beams essentially exhibited the same behavior as observed before strengthening. Therefore, the discussion in the following sections focuses primarily on the strengthened specimens, while the reference specimens are included in the summary tables for completeness and comparison.

In this study, the impact strikes are numbered sequentially for clarity: the first impact is referred to as Event 1, and the 25th impact as Event 25. Throughout the figures, tables, and discussions, this convention is used for all individual impact events. The displacement curves demonstrate a range of differences between the experimental and numerical results (approximately 4% - 12%), with greater differences in Event 1, as indicated in Table 2. However, all numerical models captured the general shape of the response and the timing of the response, as shown in Figures 10 and 11.

The mid-span deflection results confirm progressive stiffness degradation under repeated impacts and a clear beneficial effect of CFRP strengthening. The numerical model reproduced these trends: at Event-1 the finite-element predictions slightly underestimated the experimental deflections (stage-1 range ≈ 6.7–9.8% underestimation; including stage-2 cases the overall range becomes 6.7–12.0% underestimation), reflecting an initially stiffer model response. At Event-25 the numerical results modestly overestimated the experimental deflections for the unstrengthened cases by about 4.3–6% (while across all cases numerical differences span from −6.9% to +6%), indicating the model's sensitivity to accumulated damage parameters and the concrete softening law. The data showed mid-span deflection growth of CFRP conditioned beams from the 25th impact as follows: between 19.2 and 23.2% confirming the effectiveness of strengthening in maintaining flexural rigidity and limiting the growth of progressive deformation.

The significant degradation shown in the unstrengthened beams and the stabilizing effect imposed by CFRP strengthening were both accurately captured by the finite element model. Due to perfect contact conditions, undamaged material properties, and the absence of microcracks caused by construction, the numerical predictions at Event-1 slightly overestimated the experimental peak impact forces by approximately 8.1–16.6% for both reference and strengthened specimens. The numerical model tended to underestimate the experimental peak forces for Event-25, with differences ranging between 6.9% to 19.6%, notably for the unstrengthened beams (Table 3). This variation shows that the numerical response is more sensitive to cumulative damage, contact stiffness degradation and concrete softening over time under

repeated impacts. These differences are explained by small changes in material characteristics, boundary conditions, and intrinsic experimental uncertainties that are difficult to accurately simulate in the numerical model. Overall, the rate of impact-force degradation was significantly slowed down by CFRP strengthening, which limited the force reduction to about 31% as compared to declines in the unstrengthened beams that exceeded 36%. Further indication that the CFRP layer stabilized the global dynamic response by limiting cracking, distributing impact loads, and maintaining stiffness under repeated impact loading comes from the improved agreement between experimental and numerical responses following strengthening. The strengthened beams were able to retain higher force levels throughout the impact sequence, demonstrating improved energy absorption and provided a more stable dynamic response.

Relative to the experimental reaction-force response measurements, the peak values obtained by the numerical model approximately differed by 6.1 - 53.6%, with the largest deviation being recorded in Event-1 (Table 4). These significant discrepancies were expected during the first impact event of dynamic loading applications, as the reaction force is extremely sensitive to support compliance. On the contrary, in the finite-element modeling, the supports have been modeled as rigid elements; however, the experimental setup inevitably involved some degree of flexibility in addition to some energy-dissipation capability at the support. Consequently, the reaction force predicted by the numerical model exceeded the experimental values during the first impact.

As the number of impacts increased, the peak reaction forces obtained through numerical modelling and experimental testing exhibited a clear tendency toward convergence. By Event 25, the discrepancies between the experimental peak reaction forces and the numerical modelling were significantly reduced (approximately 6.1 - 20.6%) indicating that the numerical model captured both the progressive stiffness degradation as well as damage accumulation in the beams. This convergence confirms the stability of the numerical formulation and its ability to reproduce the degraded dynamic response under repeated impact loads.

It should be noted that the experimental reaction-force data reported in the reference study were limited. Only a single reaction-force time-history curve was provided for the first impact before strengthening, while all other impacts were reported only with peak reaction-force values and no time-history graphs showing the time-history reaction force values. Due to the limited experimental dataset available after CFRP strengthening, direct validation of the reaction-force response in Stage 2 was not possible. In the reference experimental study, the measured responses after strengthening were limited mainly to the impact force and mid-span deflection, whereas reaction-force records were not reported either as time-history curves or as peak values. Therefore, the finite-element model after strengthening was validated primarily using the experimentally available responses, namely the impact force and mid-span deflection. The reaction-force results after strengthening were consequently treated as numerical predictions obtained from the validated model and were used to interpret the load-transfer mechanism and the influence of CFRP strengthening on the dynamic response, rather than as direct experimental–numerical comparisons.

For these reasons, the reaction forces are being provided in table form (Table 4) only, while the majority of the validation numerically from this study is based on the responses of impact forces and deflections at mid-span, for which complete and consistent records were available from experiments.

The data comparing the response forces from numerical and experimental means showed that there are clear improvements in the overall dynamic response for the CFRP strengthened elements when compared to the non-CFRP strengthened elements. Based on the numerical, the reduction in peak-reaction force for the unstrengthened beams represents a considerable decrease of roughly 54.7–57.3% from Event 1 to Event 25 due to a combination of cumulative stiffness loss, accumulation of damage and deterioration of load-transfer capacity through the supports. In contrast, after CFRP strengthening; the reductions in peak-reaction force for the CFRP strengthened beams are significantly less severe, with reductions of only approximately 36.9–39% during the same event sequence. The reduction in the rate of degradation corresponds to an increase in the stiffness of the CFRP-strengthening enhanced beams such that these strengthened beams had much greater stability in the reaction forces acting on them, and they were able to withstand more repeated impact without suffering significant deterioration. Thus, the strengthened (CFRP) beams are able to sustain a higher level of reaction force for longer in their impact histories, thereby supporting the premise that CFRP is effective in maintaining the integrity of the global load transfer system.

This approach confirms a reliable and meaningful assessment of the numerical model while acknowledging the limitations of the available experimental reaction-force result. The strong correlation between the numerical and experimental response for these beams substantiates the reliability of the numerical model as a means to predict the dynamic response of the beams, therefore allowing for its application to other evaluations.

4.1. Reaction and Inertia Force Analysis Before and After CFRP Strengthening

The inertia force represents the portion of the impact load consumed in accelerating the beam mass and internal vibration modes and therefore provides a direct indicator of the dynamic demand imposed on the structure. In a structural system that has been subjected to repeated loading from impacts, the relationship of the reaction force to the inertia force provides an important indication of both how much dynamic energy has been transferred and how much of the mass has participated in those dynamic loads.

The inertia force is evaluated from the equilibrium relation.

$$F_{impact}(t) = F_{reaction}(t) + F_{inertia}(t) \quad (1)$$

which gives;

$$F_{inertia}(t) = F_{impact}(t) - F_{reaction}(t) \quad (2)$$

In the current study, the behavioral differences of beams before and after carbon fiber reinforced polymer (CFRP) strengthening were examined. Beams SB1-CS-D and SB2-CS-D exhibited a nonlinear decrease in reaction force with increasing impact number, reflecting a reduced capacity to transfer loads to the supports due to accumulated damage, including cracking, local buckling, and loss of stiffness (Figures 12 and 13). These findings are consistent with Li et al. (2015) [50], who reported that damage accumulation and microcrack propagation cause concrete elements subjected to impact loads to gradually lose stiffness.

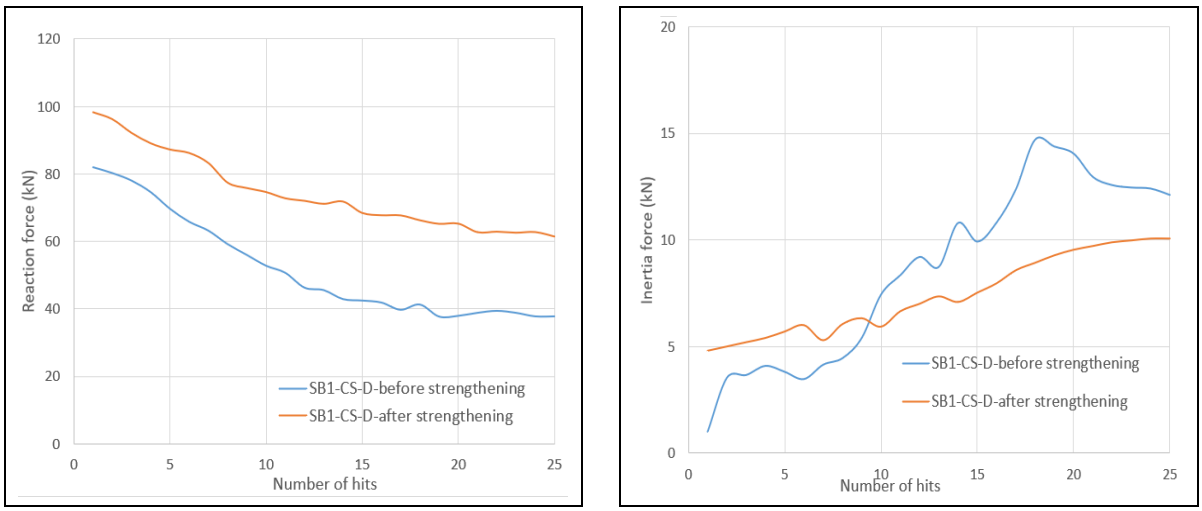

Figure 12. Reaction and inertia forces for specimen SB1-CS-D

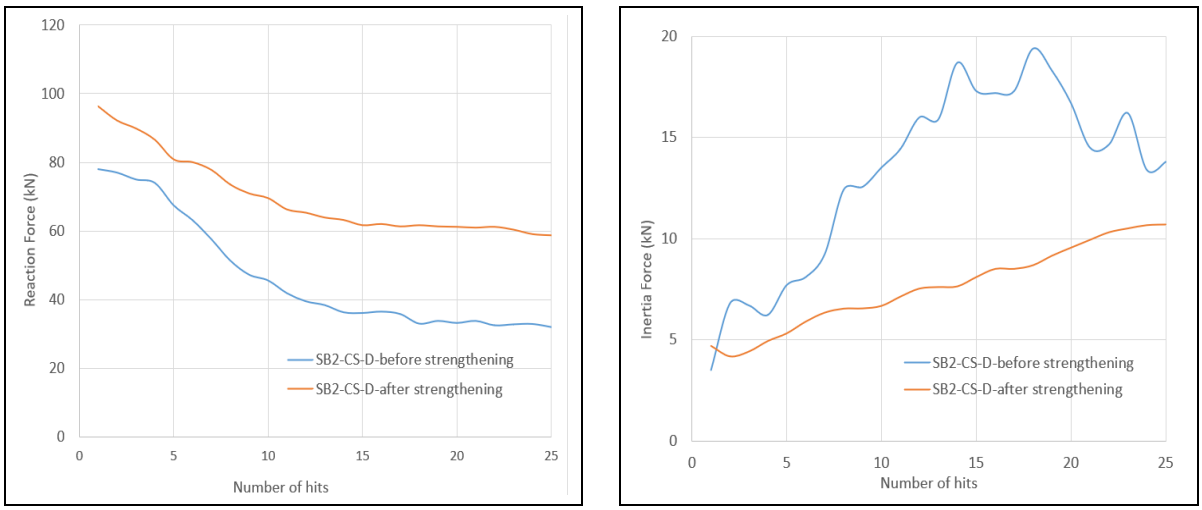

Figure 13. Reaction and inertia forces for specimen SB2-CS-D

The inertia-force response exhibited larger discrepancies between experimental estimates and numerical predictions compared with the impact and reaction forces (Table 5). Inertia forces were therefore analyzed primarily in terms of relative trends rather than absolute agreement. In this study, the inertia force was evaluated from the equilibrium relation between the impact force and the reaction force. Therefore, the inertia-force value is highly sensitive to any discrepancy in either the impact-force or reaction-force response, particularly the reaction force response. Consequently, the calculated inertia force becomes sensitive to the prediction of the reaction force. As discussed previously for Table 4, the relatively large reaction-force discrepancy at the first impact event was mainly associated with the idealized support and contact conditions in the numerical model. This discrepancy directly affected the calculated inertia force and explains the larger numerical–experimental differences observed in Table 5. Before strengthening, the numerical calculations used to generate inertia force data were much lower than those from the experimental tests. The differences

between numerical calculated and experimental results were over 82.5% to 94.4% for Event-1, and from about 6.4% to 42.1% at Event-25. Although both experimental and numerical results had different absolute values, their trends were the same. The peak inertia force recorded on un-reinforced specimens decreased with each subsequent impact, indicating a change in stiffness characteristics due to the accumulated damage within the concrete specimen (through deterioration), as well as a decrease in acceleration and an increase in energy dissipation with continued application of load. It rose to 8.1–10.8 kN, corresponding to an increase of approximately 523% and 237.5% relative to the first impact after 18 events before stabilizing. This suggests that the specimens had reached a maximum level of cumulative damage and associated loss of stiffness.

Table 5. Inertia force; experimental and numerical data

Specimens ID	Inertia Force (kN)									
	Stage-1 (before strengthening)						Stage-2 (after strengthening)			
	Experimental data		Numerical data		Difference%		Experimental data		Numerical data	
	Event-1	Event-25	Event-1	Event-25	Event-1	Event-25	Event-1	Event-25	Event-1	Event-25
SB1-US-D	17.78	13.98	1.3	8.1	-92.7	-42.1				
SB1-CS-D	17.80	13.12	1.0	11.9	-94.4	-9.3	N/A	N/A	4.50	10.0
SB2-US-D	18.30	12.96	3.2	10.8	-82.5	-16.7				
SB2-CS-D	18.28	14.74	3.5	13.8	-80.9	-6.4	N/A	N/A	4.8	10.3

The numerical inertia forces exhibited an increase in magnitude and stability in successive impacts after being strengthened with CFRP, indicating an improved ability to retain stiffness and provide a more consistent response to dynamic loading. These numerical inertia forces remained relatively low (4.5–10.3 kN at Event-22) after being strengthened by CFRP, although they increased compared to the first impact (approximately 114.6–122.2%) because of the small magnitudes of inertia forces at the time of first impact; however, the overall inertia response remained limited, indicating that CFRP strengthening not only decreased the amplification of acceleration but also reduced the inertial effects caused by repeated impact loads. In addition, the CFRP sheets enhanced the stiffness retention and dynamic energy dissipation characteristics, indicating that the CFRP strengthening system limited excessive dynamic deformations of the beams during repeated impacts and limited the development and progression of localized damage. These characteristics of stabilized inertial force response are consistent with the moderated decrease in impact-force degradation, reaction forces, and restrained mid-span deflections that were observed following the CFRP strengthening. In general terms, although direct quantitative agreement between experimental and numerical inertia forces is limited due to differences in how inertia is evaluated. The primary use of the finite-element models was to simulate general dynamic behavior. As such, the inertia force results were used mainly to evaluate the stability of structural responses, the stiffness evolution, and the effectiveness of CFRP strengthening, rather than as a strict metric for numerical validation.

In general, for SB1 specimens with slender webs ($h_w/b_w = 4.33$), it was found that the numerical peak reaction force decreased by 54.7% before strengthening and by 36.9% after CFRP strengthening. The gradual reduction in beam stiffness indicates that cracks have built up over time, causing localized damage and reducing the ability of the beams to carry loads through to their supports. In terms of absolute improvements in reaction forces before and after CFRP application, the average improvements were 17.8%. SB2 specimens, with webs closer to compact behavior ($h_w/b_w = 3$), exhibited slightly larger reductions of 57.3% before strengthening and 39.0% after CFRP strengthening, yielding an absolute improvement of 18.3 percentage points, which indicates that the CFRP layer has improved the load-carrying capacity and assisted in maintaining the structural stiffness of the beams. "Percentage points" refers to the absolute difference in reaction force reduction from before CFRP and after CFRP applications.

These results show a marginally higher strengthening efficiency in SB2 in relative terms, whereas SB1 retained a higher absolute reaction force capacity after strengthening. Furthermore, given identical reinforcement layouts, the observed differences confirm the influence of the web's slenderness on stiffness degradation. SB1 had greater overall stiffness, and SB2 had a more rapid decline in stiffness with repeated impact loading. In SB2, the inertia force had greater values, suggesting a larger difference between the impact forces and the reaction forces. In summary, SB1 was more global in resistance, maintaining overall stiffness despite greater susceptibility to local buckling, whereas SB2 was weaker and degraded faster. CFRP (Carbon Fiber Reinforced Polymer) is a type of externally bonded material that can improve the strength and stability of concrete members, according to the latest published standards (ACI PRC 440.2:2023 [51]). Increasing the stiffness, preserving the cracking, and increasing the level of energy dissipation through external bonding result in less oscillation of the beam and inertia response became more controlled. It is also worth

noting that the reference specimens (SB1-US-D and SB2-US-D), which were tested under 25 impacts events only, showed very similar trends in reaction force degradation and inertia values compared to the primary beams before strengthening. Therefore, these results are not presented here so as not to create duplicate data.

4.2. Residual Capacity of Beams Subjected to Repeated Impacts

Residual capacity is a measure of how well beams that have suffered impacts maintain their structural integrity when subjected to multiple impacts. This study uses the Residual Performance Index (RPI) to determine the remaining load-transfer capacity expressed as a percentage of its initial load-carrying capacity following a specified number of impact events. The RPI is a dimensionless ratio that shows how a material responds during a specific impact event to the corresponding value at the initial time, before any damage occurred. Any values close to one will indicate that the material has only experienced minor deterioration, whereas lower values will show more severe loss of stiffness and increase in total/overall damage. Thus, RPI reflects how much of the original structural performance is still preserved.

Residual performance of unstrengthened beams and CFRP-strengthened beams has been studied based on how they evolve after an impact event. Web slenderness, damage propagation after impact, and external reinforcement all have an influence on residual performances.

$$RPI = \frac{F_i}{F_1} \tag{3}$$

where, *RPI* refers to the value of the residual performance index, based on the peak impact or reaction-force data; F_i- is the peak impact or reaction force at impact event i; F_1- is the peak impact or reaction force at first impact event (the baseline condition).

The performance of the system, for both impact and reaction forces was evaluated for reinforced concrete beams SB1 and SB2 before and after CFRP strengthening (Tables 6 and 7). The results reveal two distinct behavioral phases, as illustrated in Figure 14.

Table 6. Residual performance index based on the peak impact

Specimens ID	Before strengthening peak impact (kN)				After strengthening peak impact (kN)			
	F_1	F_{25}	F_{25}/F_1	Reduction	F_1	F_{25}	F_{25}/F_1	Reduction
SB1-US-D	81.00	44.20	0.546	45.4%				
SB1-CS-D	83.00	49.90	0.601	39.9%	102.00	71.50	0.700	30%
SB2-US-D	81.00	44.00	0.543	45.7%				
SB2-CS-D	81.50	45.80	0.562	43.8%	101.10	69.00	0.683	31.7%

Table 7. Residual performance index based on the peak reaction

Specimens ID	Before strengthening peak reaction (kN)				After strengthening peak reaction (kN)			
	F_1	F_{25}	F_{25}/F_1	Reduction	F_1	F_{25}	F_{25}/F_1	Reduction
SB1-US-D	79.70	36.10	0.453	54.7%				
SB1-CS-D	82.00	38.00	0.463	53.7%	97.50	61.50	0.630	37.0%
SB2-US-D	77.80	33.20	0.427	57.3%				
SB2-CS-D	78.00	32.00	0.410	59.0%	96.30	58.70	0.609	39.1%

Before strengthening, progressive reductions in impact or reaction forces were observed, showing decreases of approximately 39.9%-45.7% and approximately 53.7%-59.0%, respectively, with increasing impact number. The observed decrease in both the impact and reaction forces suggests a continuous reduction in system performance due to accumulated damage; this accumulated damage was the result of localization of concrete crushes occurring at the interface bend of the L-shaped junction (ledge-web corner) and expanding flexural-shear cracks along the ledge-web interface. This indicates that the reduction in residual capacity was ruled not only by local impact damage, but also by the gradual loss of load-transfer efficiency through the ledge-web connection. It was observed that, the degradation rate of SB2 (web height = 450 mm) was significantly higher than that of SB1 (web height = 650 mm). The shorter web height in SB2 provided less rotational restraint at the ledge–web junctions, resulting in greater demand for local bending and faster loss of stiffness under repeated impact events. Therefore, the higher degradation rate of SB2 can be attributed to its geometry, which made the ledge-web region more vulnerable to crack widening and stiffness deterioration. This finding concurs with previously reported studies that state that the severity and concentration of the damage in the impact zone determine the performance of RC spandrel beams.

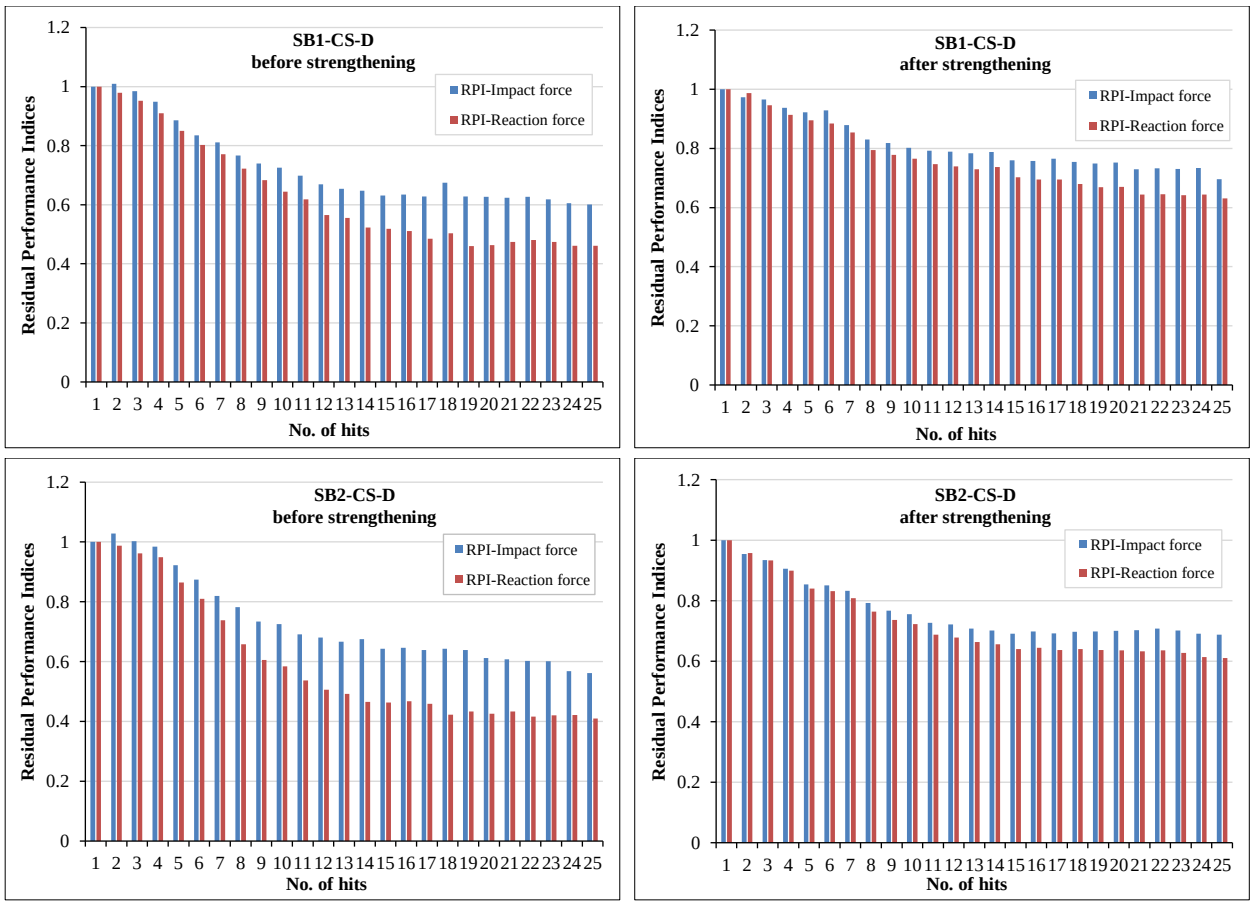

Figure 14. Residual capacity under repeated testing conditions for SB1 and SB2

After strengthening with carbon fiber sheets, the beams showed a significant increase in performance when tested in the earliest post-strengthening impacts. This improvement suggests that the CFRP sheets contributed to restoring part of the beam stiffness and improving the continuity of force transfer across the damaged region. Additionally, the rate of deterioration of the impact and reaction forces decreased significantly after the strengthening process, by 30 - 31.7% and 37 - 39.1%, respectively. CFRP's effectiveness at reducing crack width and aiding in the transfer of load between the concrete and steel reinforcement was evident here. In this sense, the CFRP acted as a crack-bridging layer, limiting further crack opening and reducing stress concentration around the damaged ledge-web interface. While there are clear differences in geometry between SB1 and SB2, the CFRP layer helped align the load path, improved strain compatibility at the ledge–web junctions, and limited torsional deformations. Therefore, both beams exhibited a more uniform and stable overall dynamic response under repeated impacts.

Moreover, after strengthening, the difference in impact-based and reaction-based residual performance indices (RPIs) is much smaller, as strengthening a structure improves its efficiency in transferring loads and reduces the internal dissipation of energy. The closer agreement between the two RPI values indicates that the strengthened beams developed a more uniform dynamic response, where the applied impact force was transferred more effectively toward the supports. In general, the beams' performance prior to strengthening behaved primarily according to their geometry and material properties, while after CFRP sheet installation the mechanical characteristics and the CFRP confinement significantly influenced beam performance. This indicates how effective CFRP has been in restoring and stabilizing beam dynamic responses under repeated impact loads.

From a practical perspective, CFRP strengthening offers several advantages for field applications, due to being low in additional weight and offering corrosion resistance and simplified installation compared to traditional methods of strengthening. Because of these advantages, it is appropriate to use CFRP for retrofitting existing reinforced concrete beam systems in order to accommodate multiple impact variations from either accidental or dynamic load applications. However, successful field application requires proper surface preparation, sufficient bonding strength, and appropriate protection of the CFRP layer against de-bonding, fire, mechanical damage, and environmental exposure are all required proper surface preparation, reliable bonding, and protection of the CFRP layer against debonding, fire, mechanical damage, and environmental exposure. Generally, Although the initial material cost of CFRP may be relatively high, its rapid installation and limited disruption to service can improve its overall constructability and practical applicability.

4.3. Comparative Analysis of Impact and Reaction Forces before and after Strengthening

An analysis was conducted to better understand the dynamic interaction between the impactor and the beams, using the time-history responses for the impact and the reaction forces on some select representative impact events (Figure

15). Accordingly, the first impact event was selected to illustrate the beams' initial, nearly elastic response before cracking or stiffness degradation, while the eighteenth impact event represents a stage where the reaction forces stabilize, indicating that the damage in the concrete is approaching a steady-state condition.

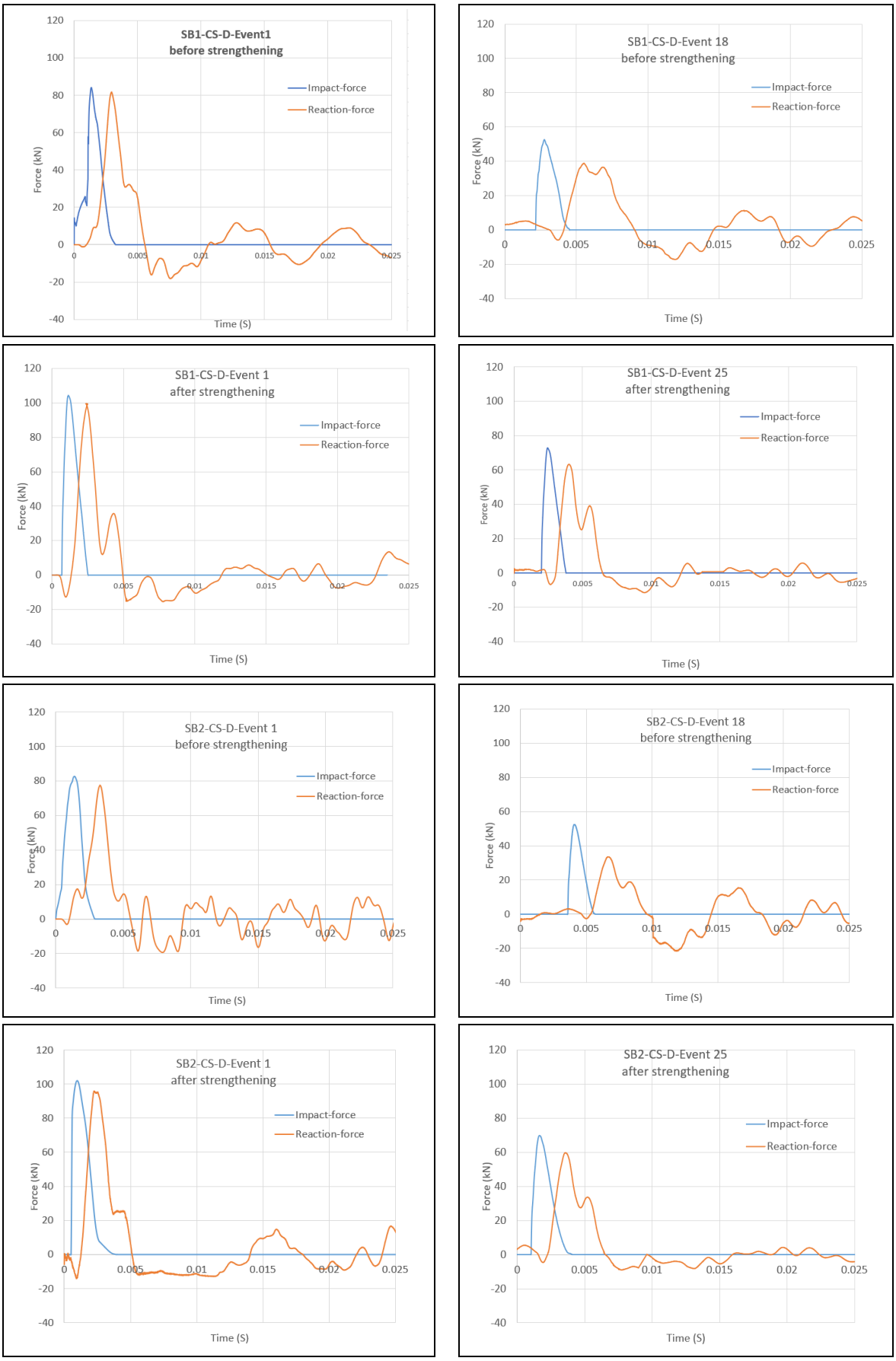

Figure 15. Impact force and reaction force time history for SB1-CS-D and SB2-CS-D

The initial and final impacts after CFRP strengthening have been used to evaluate how effective the CFRP strengthening was at restoring the original stiffness as well as reducing the accumulation of damage in the member. The corresponding impact and reaction force time-history curves for these representative events are presented and discussed to highlight changes in force magnitude, time lag, and overall dynamic response before and after strengthening.

For unstrengthened and strengthened spandrel beams, the numerical peak impact force for SB1 and SB2 spandrel beams decreased gradually with increasing impact events by 42.65% and 44.75%, respectively. Profoundly damaged concrete and steel in combination predict a gradual decrease in stiffness (deformation resistance) and a concomitant decline in the structural capacity of those beams to respond to impact loads over time. Strengthening those beams resulted in an overall improvement in the ability of those beams to respond to impact forces, the impact force increased and remained considerably more stable across repeated impacts, with the reduction in force being smaller than before strengthening. The retrofit of CFRP to both SB1 and SB2 decreased the peak numerical impact force of both beams by 29.9% and 31.8%, respectively, demonstrating that the CFRP retrofit significantly enhanced the beams' stiffness and energy-resisting capacity. The increase in both stiffness and energy-resisting capacity is due to the reinforcement and confinement effect of the CFRP layer providing supplemental confinement to help minimize crack propagation and delaying subsequent degradation of both beams after exposure to repeated-impact loads.

The performance of the beams dynamically can be characterized by the behavior of the reaction force. Initially, before strengthening, the reaction force appeared early during the first impacts, and as additional impacts occurred, this force became present later than the first impact event, indicating an increase in deterioration of the beam's loading capacity and reduced load-transfer efficiency. The average peak reaction force was reduced approximately 54.2% to 58.2% for SB1 and SB2, respectively, and shows a significant reduction in the stiffness of the specimens and the delayed dynamic response to the impact force. After strengthening, the reaction force reductions were lower (~36.9%, SB1, 39%, SB2) and consistently occurred later than the impact force. This behavior is indicative of the CFRP layer absorbing and redistributing impact energy prior to being transmitted to the support, and indicates an increased degree of structural damping and restraint [52].

Before strengthening, there was an increasing gap between the impact and reaction forces as impacts were repeatedly applied. This is attributed to continued degradation of load transfer efficiencies through progressive damage. This divergence narrowed considerably with CFRP strengthening through the 25th impact. This indicates that strengthening with CFRP assists in maintaining the structural load transfer ability, thereby lessening the probability of the occurrence of further progressive failures within the interface zone. In addition, the unstrengthened specimens showed post-peak oscillations (Figure 15) that reflected the low damping produced by the cracks and the resulting instability of the specimens' vibrations. However, after the strengthening of these specimens, the post-peak oscillations were significantly diminished. The continuous bonding between the CFRP and concrete enabled greater internal damping, therefore resulting in smoother signals, as well as minimized wave reflections within the section. In this context, the divergence and convergence behavior can be understood conceptually as a change in the load-transfer mechanism between the impact point and the supports. Originally, the divergence between the point of impact and the reaction force to that point is representative of both the time lag and energy lost during that period due to the time required to transmit that load, whereas the later narrowing of this gap indicates improved force redistribution and a more stable dynamic response after CFRP strengthening.

SB1 was able to retain more absolute stiffness due to its slender webs ($h_w/b_w = 4.33$), while SB2, with webs closer to compact ($h_w/b_w = 3$), experienced a greater rate of deterioration of reaction forces. After the addition of CFRP strengthening, both beams showed similar increase in impact forces, but SB2 exhibited a slightly larger relative gain in reaction-force retention. The results of these observations demonstrate that both the slenderness of the web and the application of CFRP to strengthen it are significant factors with respect to the residual dynamic performance of a beam.

The results also indicate that not only do CFRP applied to the beam enhance the peak force capacity of the beam, but they also provide additional stabilization to the beam's dynamic performance; provide improved load transfer efficiencies, and increase the ability of the beam to withstand progressive damage through repeated impact events.

4.4. Time-History Analysis of Midspan Deflection

The current research utilized a cumulative simulation framework where the damage and residual deflection from each impact were carried forward into the next impact using Abaqus's initial state feature. Accordingly, the new impact started at the deformation accumulated from the previous impacts. Under cyclic loading conditions, this method is realistic since it accounts for the fact that after repeated impacts, the geometry of the beam does not completely revert back to its pre-impact state. The behavior of the beam becomes path-dependent, meaning that its response during any given impact is governed not only by the current load but also by the full loading history of all previous cycles as well as the total damage that has occurred throughout the sequence.

The post-processing step removed the portion of the residual deflection of the previous impact responses to allow for a direct comparison with the reference study, and then all curves were re-zeroed so that they all started from zero. This normalization of the curves was strictly for presentation purposes in order to be able to create similar and comparable plots. The underlying numerical model still fully accounted for the cumulative residual deflection and damage continuity throughout all impacts as well as their progression through time, meaning that the structural history and progressive degradation remained embedded in the simulation despite the graphical re-scaling.

Before strengthening, the mid-span deflection continued to grow with each successive impact to approximately the 18th hit, when the deflections began to stabilize, indicating that the beam had reached a damage-saturation stage. For this reason, the 1st and 18th impacts were selected for comparison in the deflection analysis, as they effectively capture the transition from the initial elastic response to the stabilized damage state. The results show a clear reduction in maximum mid-span deflection following CFRP strengthening. For example, the peak deflection at the 25th impact decreased by approximately 19.2% for SB1 and 23.2% for SB2 compared to the unstrengthened beams. This reduction confirms the enhanced stiffness and improved structural integrity provided by the CFRP retrofit (see Figure 16).

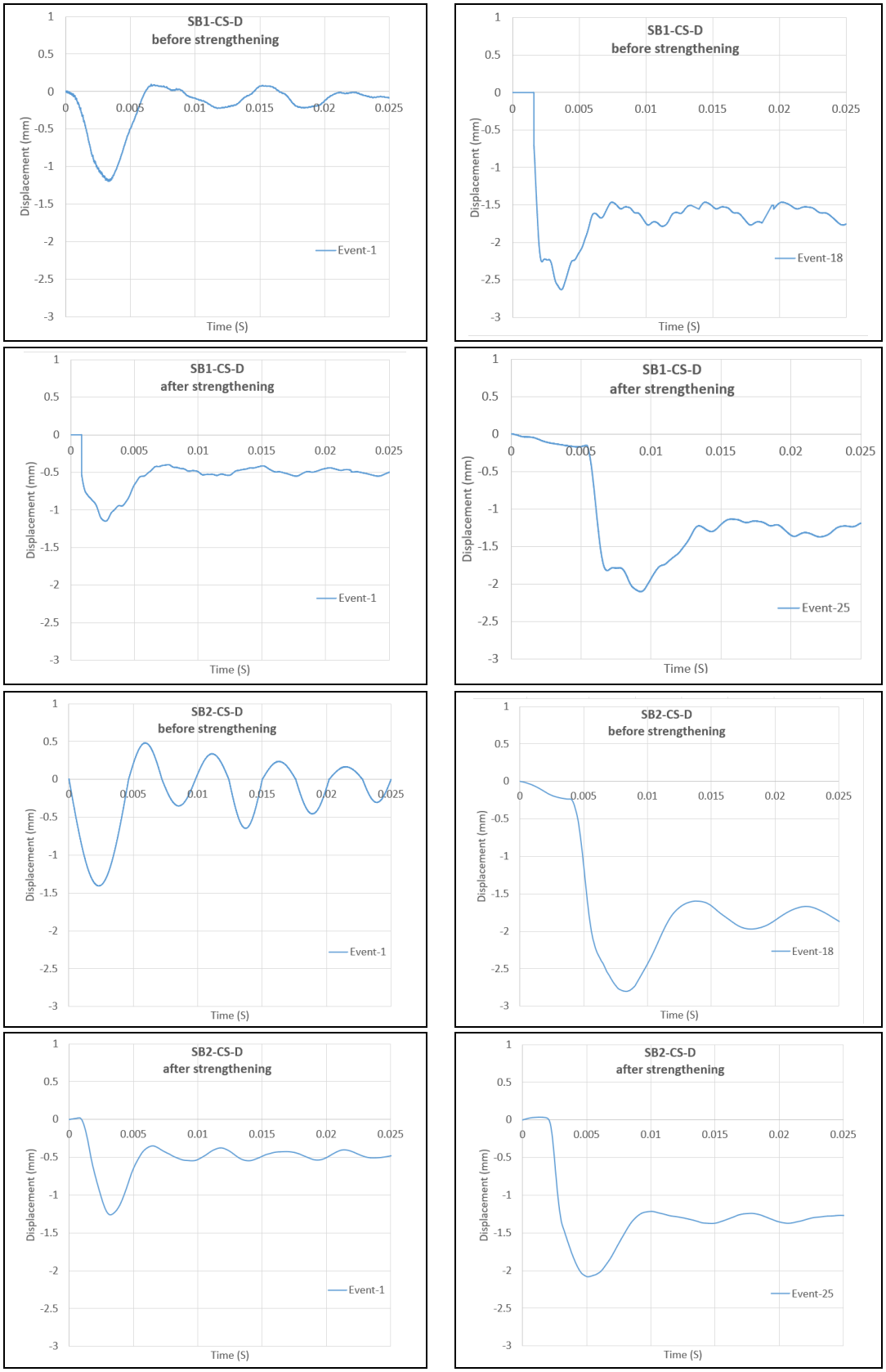

Figure 16. Displacement-time history for SB1-CS-D and SB2-CS-D

4.5. Impact-Induced Damage Evolution in Concrete Beams before and after CFRP Strengthening

Before strengthening, the evolution of tensile damage in the concrete, as quantified by the DAMAGET variable in Abaqus, was evaluated at impacts 1, 10, and 25 to characterize degradation mechanics under repeated loading. At first, damage was confined to a narrow zone beneath the impact point, corresponding to the initial flexural-tensile cracking induced by the localized stress concentration. By the 10th strike, the damaged region had expanded both vertically and longitudinally along the tensile face, reflecting the formation and coalescence of multiple microcracks. This expansion corresponds to a progressive reduction in local stiffness, increasing curvature demand and redistributing tensile stresses away from the impact zone toward the beam extremities.

By the 25th impact, the DAMAGET index approached values indicative of near-complete tensile degradation, signifying that the crack network had reached a density at which the concrete could no longer contribute meaningfully to tensile resistance. At this stage, the beam behaved as an extremely damaged flexural member with significantly reduced energy-absorption ability, depending primarily on the steel reinforcement bars to sustain repeated impacts. Once tensile damage has saturated, the system's behavior transitions from progressive stiffness deterioration to a quasi-steady state, with an emphasis on residual deformations and reinforcement-controlled behavior.

After strengthening, since the damages in the concrete had already achieved a near-saturated state, the attention was focused on how the CFRP strengthening would react to successive impact loading. Hashin failure criteria were utilized within the Abaqus finite element model to track intra-laminar damage mechanisms, distinguishing fiber and matrix failures in tension and compression. Throughout the entire duration of the post-retrofit impacts, all damage indices associated with the fibers consistently remained at a value less than 0.1, indicating that the carbon fibers retained their tensile-load-carrying capability and did not approach fracture.

Using damage visualization in Abaqus, the matrix tensile damage (HSNMTCRT) due to impact events 1, 10 and 25 was evaluated. The results indicated that localized matrix microcracks began to occur early, followed by progressive expansion with each of the subsequent impacts. From a fracture mechanics perspective, this microcracking represents gradual deterioration of the resin in addition to being the start of local fiber–matrix debonding (Figure 17), while also serving as controlled-energy dissipation sites, absorbing some of the energy before it can be transferred to the fibers. This process introduces reductions that occur in local stiffness within the laminate, changes in stress-transfer mechanisms between fibers, and redistribution of high loads to surrounding undamaged fibers, as captured by the incremental stiffness matrices in the Abaqus solver.

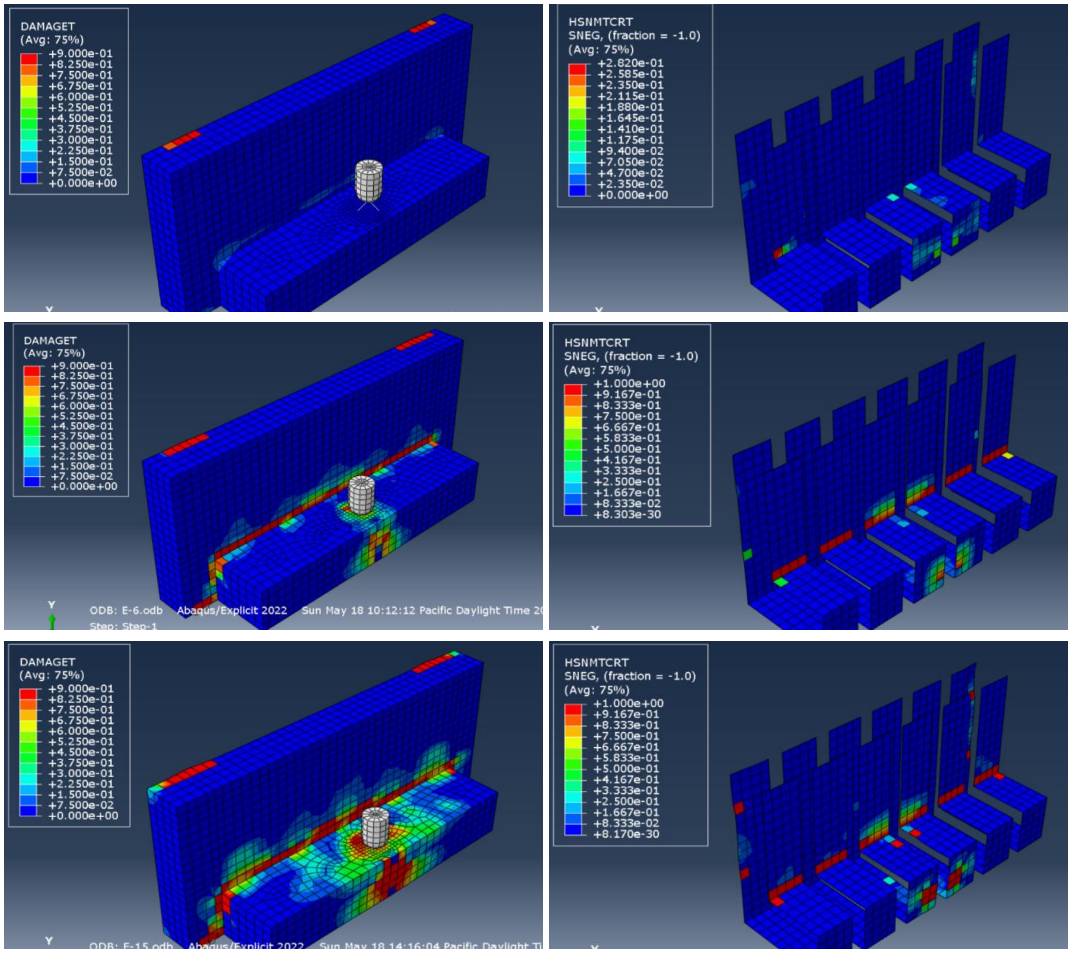

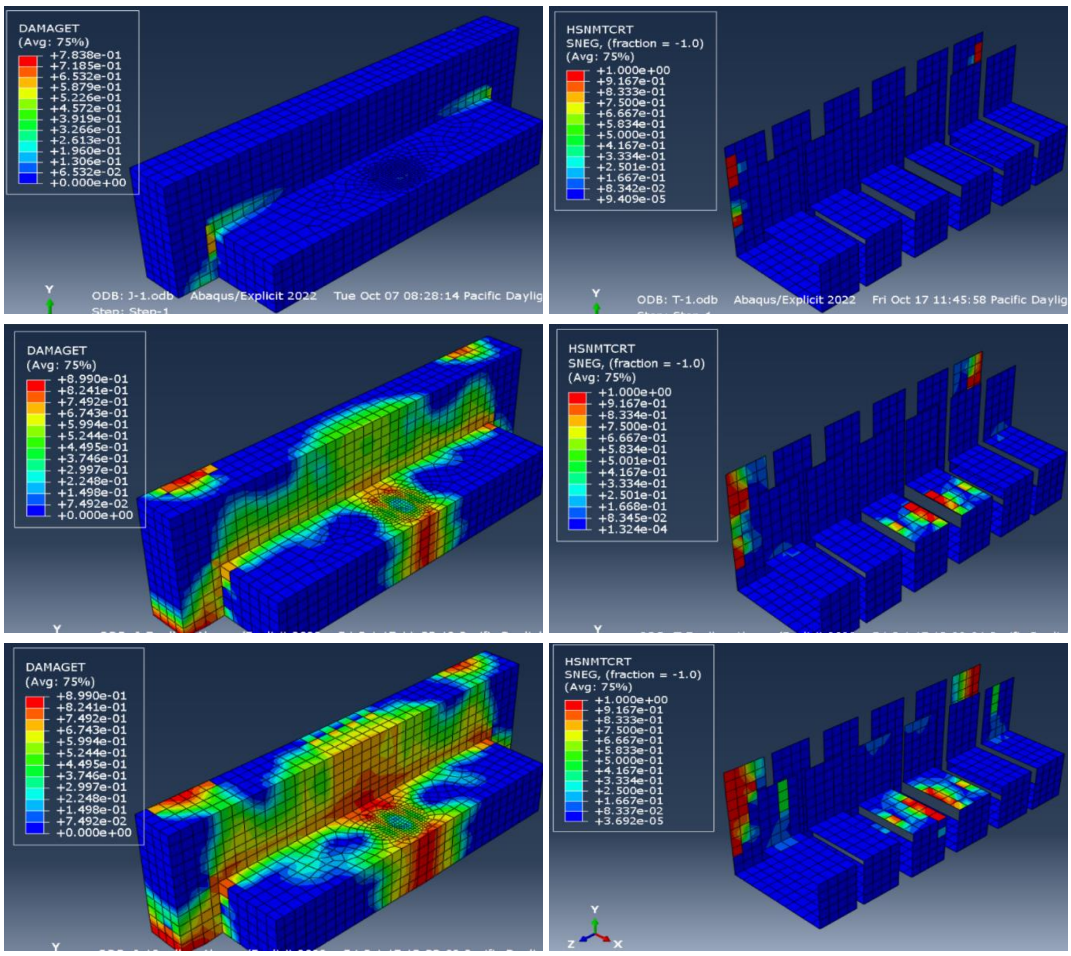

Figure 17. Concrete and CFRP damage patterns before and after strengthening under repeated impacts

The test results demonstrate no evidence that any impact stress exceeded the tensile failure level of the carbon fibers, confirming the high effectiveness of the CFRP system. The matrix serves as the main layer responsible for energy and stress absorption, increasing the time delay in transferring energy to the carbon fibers and thereby reducing the likelihood of energy transfer and sudden failure. CFRP matrix damage is an early indication of structural deterioration, while the absence of fiber tensile failure (DAMAGEFT) up to the 25th impact demonstrates that the CFRP not only significantly improved the beam's ability to withstand repeated impact loads but also helped stabilize the beam's dynamic response and delay the occurrence of progressive structural failure.

This approach highlights the progressive transfer of damage from the concrete to the CFRP strengthening sheet and clarifies the post-retrofit failure mechanism. These findings are consistent with those of Youbi et al. (2022) [53] and Alobaidi & Al-Zuhairi (2023) [54]. The damage growth observed in both the fiber and the matrix, as captured through the Abaqus damage variables, corresponds with the mechanical performance, showing a clear increase in impact resistance, improved load-transfer efficiency, and reduced deflection growth under repeated impacts.

5. Conclusion

The present study numerically investigated the repeated-impact response of L-shaped reinforced concrete (RC) spandrel beams before and after strengthening with externally bonded CFRP sheets. A validated ABAQUS finite element model was used to capture impact forces, reaction forces, inertia forces, deflections, and damage development.

The impact resistance of L-shaped beams under repeated mid-span impacts was significantly enhanced by CFRP strengthening. In the unstrengthened beams, the reduction in peak impact force over 25 impacts was almost 45%, whereas in the strengthened beams, it ranged between 29.9% and 31.8%. A similar improvement was observed in the reaction-force response. Before strengthening, the reaction force decreased by approximately 54.7%–57.3% between the first and 25th impacts. After CFRP strengthening, the reduction was limited to approximately 36.9%–39%, demonstrating the effectiveness of CFRP in preserving load-transfer capacity and delaying stiffness deterioration under repeated impacts. In addition, the inertia-force response became more stable after CFRP strengthening, indicating improved dynamic stability and a more controlled acceleration response under repeated impact loading.

The increase in mid-span deflection from the first to the 25th impact was approximately 90% for the unstrengthened beams, whereas the CFRP-strengthened beams exhibited significantly lower increases in mid-span deflection: 60% for SB1-CS-D and 65% for SB2-CS-D. The finite element model reproduced the trend of the experimental deflection with acceptable differences at both the first and final impact events. In addition, after CFRP strengthening, the maximum mid-span deflection at the 25th impact decreased by approximately 19.2% for SB1 and 23.2% for SB2, indicating improved structural integrity and reduced progressive deformation.

The residual performance index (RPI) confirmed that beams strengthened with CFRP maintained a higher proportion of their original load-carrying capacity, with lower reductions in both impact-force and reaction-force performance. According to the damage evolution analysis, concrete tensile cracking propagated intensively and approached a near-saturation state by the 25th impact in the unstrengthened beams. In the strengthened beams, however, fiber tensile damage remained negligible, with DAMAGEFT < 0.1, indicating the effectiveness of CFRP strengthening in controlling crack propagation and absorbing impact energy. Overall, these findings confirm that externally bonded CFRP sheets improve the repeated-impact performance of RC spandrel beams by reducing force degradation, limiting deformation growth, enhancing energy dissipation, stabilizing the dynamic force response, and delaying damage accumulation.

6. Declarations

6.1. Author Contributions

Conceptualization, N.O.; methodology, N.O. and E.M.M.; formal analysis, N.O., E.M.M., and A.A.A.; investigation, N.O., E.M.M., and A.A.A.; data curation, N.O., E.M.M., and A.A.A.; writing—original draft preparation, E.M.M., A.A.A., and N.O.; writing—review and editing, E.M.M. and A.A.A. All authors have read and agreed to the published version of the manuscript.

6.2. Data Availability Statement

The data presented in this study are available on request from the corresponding author.

6.3. Funding

The authors received no financial support for the research, authorship, and/or publication of this article.

6.4. Conflicts of Interest

The authors declare no conflict of interest.

7. References

[1] Raths, C. H. (1984). Spandrel Beam Behavior and Design. PCI Journal, 29(2), 62–131. doi:10.15554/pcij.03011984.62.131.

[2] Cleland, N. M., & Baber, T. T. (1986). Behavior of Precast Reinforced Concrete Ledger Beams. PCI Journal, 31(2), 96–117. doi:10.15554/pcij.03011986.96.117.

[3] Logan, D. R. (2007). L-spandrels: Can torsional distress be induced by eccentric vertical loading? PCI Journal, 52(2), 46–60. doi:10.15554/pcij.03012007.46.61.

[4] Ali, A. A. M. (1983). Strength and behaviour of reinforced concrete spandrel beams. Ph.D. Thesis, University of Edinburgh, Edinburgh, Scotland.

[5] Lucier, G., Rizkalla, S., Zia, P., & Klein, G. (2007). Precast concrete, L-shaped spandrels revisited: Full-scale tests. PCI Journal, 52(2), 62–76. doi:10.15554/pcij.03012007.62.76.

[6] Hassan, T., Lucier, G., Rizkalla, S., & Zia, P. (2007). Modeling of L-shaped, precast, prestressed concrete spandrels. PCI Journal, 52(2), 78–92. doi:10.15554/pcij.03012007.78.92.

[7] Mercan, B., Schultz, A. E., & Stolarski, H. K. (2010). Finite element modeling of prestressed concrete spandrel beams. Engineering Structures, 32(9), 2804–2813. doi:10.1016/j.engstruct.2010.04.049.

[8] Salman, R., & Ali, A. (2015). Reinforced Concrete Spandrel -Floor Beams Interaction. International Journal of Innovative Research in Science, Engineering and Technology, 4(6), 3793–3800.

[9] Hussein, P. A., Nabil, M., & El-Deen, E. (2017). Contribution of Inner Stirrups With the. Al-Azhar University Civil Engineering Research Magazine (CERM, 39(39), 245–262.

[10] Wilden, H. (2010). PCI Design Handbook: Precast and Prestressed Concrete. Precast/Prestressed Concrete Institute, Chicago, United States.

[11] ACI 318-14. (2014). Building Code Requirements for Structural Concrete and Commentary. American Concrete Institute (ACI), Farmington Hills, United States.

[12] Hariharan, V., Lucier, G., Rizkalla, S., Zia, P., Klein, G., & Gleich, H. (2019). Behavior Of Compact L-Shaped Spandrel Beams with Alternative Web Reinforcement. PCI Journal, 64(2), 39–54. doi:10.15554/pcij64.2-04.

[13] Pham, T. M., & Hao, H. (2016). Review of Concrete Structures Strengthened with FRP Against Impact Loading. Structures, 7, 59–70. doi:10.1016/j.istruc.2016.05.003.

[14] Salom, P. R., Gergely, J., & Young, D. T. (2004). Torsional retrofit of spandrel beams with composite laminates. Proceedings of the Institution of Civil Engineers: Structures and Buildings, 157(1), 69–76. doi:10.1680/stbu.2004.157.1.69.

[15] Salom, P. R., Gergely, J., & Young, D. T. (2004). Torsional Strengthening of Spandrel Beams with Fiber-Reinforced Polymer Laminates. Journal of Composites for Construction, 8(2), 157–162. doi:10.1061/(asce)1090-0268(2004)8:2(157).

[16] Al-Rousan, R., & Abo-Msamh, I. (2019). Bending and torsion behaviour of CFRP strengthened RC beams. Magazine of Civil Engineering, 92(8), 48–62. doi:10.18720/MCE.92.4.

[17] Al-Rousan, R., & Abo-Msamh, I. (2020). Impact of anchored CFRP on the torsional and bending behaviour of RC beams. Magazine of Civil Engineering, 96(4), 79–93. doi:10.18720/MCE.96.7.

[18] Askandar, N. H., & Mahmood, A. D. (2020). Torsional Strengthening of RC Beams with Continuous Spiral Near-Surface Mounted Steel Wire Rope. International Journal of Concrete Structures and Materials, 14(1), 7. doi:10.1186/s40069-019-0386-4.

[19] Alzabidi, S. M., Diaa, G., Abadel, A. A., Sennah, K., & Abdalla, H. (2023). Rehabilitation of reinforced concrete beams subjected to torsional load using ferrocement. Case Studies in Construction Materials, 19, 2433. doi:10.1016/j.cscm.2023.e02433.

[20] Ayaad, N., & Oukaili, N. (2023). Efficiency of CFRP torsional strengthening technique for L-shaped spandrel reinforced concrete beams. Journal of the Mechanical Behavior of Materials, 32(1), 20220243. doi:10.1515/jmbm-2022-0243.

[21] Ayaad, N., & Oukaili, N. (2023). Effectiveness of embedded through-section technique in strengthening reinforced concrete spandrel beams. Results in Engineering, 18, 101062. doi:10.1016/j.rineng.2023.101062.

[22] Ayaad, N., & Oukaili, N. (2023). Impact torsional behavior and strengthening of reinforced concrete spandrel beams. Case Studies in Construction Materials, 19, 2591. doi:10.1016/j.cscm.2023.e02591.

[23] Kawarai, T., Komuro, M., & Kishi, N. (2025). Low-Velocity Impact-Load-Carrying Behavior of Reinforced Concrete Beams Strengthened in Flexure by Bonding a Carbon Fiber-Reinforced Polymer Sheet to the Tension-Side Surface. Buildings, 15(10), 1713. doi:10.3390/buildings15101713.

[24] Saad, A. G., Sakr, M. A., Khalifa, T. M., & Darwish, E. A. (2025). CFRP Strengthening of RC Beams with Openings Under Impact Loads. International Journal of Concrete Structures and Materials, 19(1), 95. doi:10.1186/s40069-025-00837-6.

[25] Homayoonifar, A., Momeni, M., Hadianfard, M. A., & Bedon, C. (2026). Investigating Different Patterns of CFRP Sheets in Strengthening RC Panels Under Repeated Drop-Weight Impact Loads: An Experimental Study. Iranian Journal of Science and Technology, Transactions of Civil Engineering. doi:10.1007/s40996-025-02117-5.

[26] Duan, L., Zhang, Y., Yan, L., Bao, S., Liu, H., & Lu, J. (2025). Investigation on the crack development behaviour of CFRP strengthened RC beams under static and impact loading. Engineering Failure Analysis, 171, 109369. doi:10.1016/j.engfailanal.2025.109369.

[27] Luo, J., Zhang, J., Mao, B., Zhang, X., Ma, J., & Wu, J. (2026). Impact and post-impact performance of RC beams strengthened with near-surface mounted CFRP strips: Experimental and numerical evaluation. Structures, 86, 111452. doi:10.1016/j.istruc.2026.111452.

[28] Schaeffer, D. M. (1966). The effect of combined torsional and bending loads on a channel beam with one end restrained from warping. Master Thesis, Missouri University of Science and Technology, Rolla, United States.

[29] Mogbo, N. C. (1968). Torsional behavior of spandrel beams. Master Thesis, Rice University, Houston, United States.

[30] Klein, G. J. (1986). Design of Spandrel Beams. PCI Journal, 31(5), 76–124. doi:10.15554/pcij.09011986.76.124.

[31] Lucier, G., Walter, C., Rizkalla, S., Zia, P., & Klein, G. (2011). Development of a rational design methodology for precast concrete slender spandrel beams: Part 1, experimental results. PCI Journal, 56(2), 88–112. doi:10.15554/pcij.03012011.88.112.

[32] Lucier, G., Walter, C., Rizkalla, S., Zia, P., & Klein, G. (2011). Development of a rational design methodology for precast concrete slender spandrel beams: Part 2, analysis and design guidelines. PCI Journal, 56(4), 106–133. doi:10.15554/pcij.09012011.106.133.

[33] Zia, P., & Hsu, T. T. C. (2004). Design for torsion and shear in prestressed concrete flexural members. PCI Journal, 49(3), 34–42. doi:10.15554/pcij.05012004.34.42.

[34] ACI 318-11. (2011). Building Code Requirements for Structural Concrete and Commentary. American Concrete Institute (ACI), Farmington Hills, United States.

[35] ACI 318-19. (2014). Building Code Requirements for Structural Concrete and Commentary. American Concrete Institute (ACI), Farmington Hills, United States.

[36] ABAQUS (2022). ABAQUS Version 2022, Dassault Systèmes Simula Corp, Waltham, United States.

[37] Dassault Systèmes. (2022). Abaqus Analysis User's Manual Version 2022. Dassault Systèmes Simula Corp, Waltham, United States.

[38] Lubliner, J., Oliver, J., Oller, S., & Oñate, E. (1989). A plastic-damage model for concrete. International Journal of Solids and Structures, 25(3), 299–326. doi:10.1016/0020-7683(89)90050-4.

[39] Lee, J., & Fenves, G. L. (1998). Plastic-Damage Model for Cyclic Loading of Concrete Structures. Journal of Engineering Mechanics, 124(8), 892–900. doi:10.1061/(asce)0733-9399(1998)124:8(892).

[40] Fedoroff, A., & Calonius, K. (2020). Using the Abaqus CDP model in impact simulations. Rakenteiden Mekaniikka, 53(3), 180–207. doi:10.23998/rm.79723.

[41] Jiang, H., Wang, X., & He, S. (2012). Numerical simulation of impact tests on reinforced concrete beams. Materials & Design, 39, 111–120. doi:10.1016/j.matdes.2012.02.018.

[42] Lin, S. C., Li, D., & Yang, B. (2019). Experimental study and numerical simulation on damage assessment of reinforced concrete beams. International Journal of Impact Engineering, 132, 103323. doi:10.1016/j.ijimpeng.2019.103323.

[43] Silva, L. M. E., Christoforo, A. L., & Carvalho, R. C. (2021). Calibration of concrete damaged plasticity model parameters for shear walls. Revista Materia, 26(1), 12944. doi:10.1590/s1517-707620210001.1244.

[44] Rainone, L. S., Tateo, V., Casolo, S., & Uva, G. (2023). About the Use of Concrete Damage Plasticity for Modeling Masonry Post-Elastic Behavior. Buildings, 13(8), 1915. doi:10.3390/buildings13081915.

[45] Hordijk, D. A. (1992). Tensile and tensile fatigue behaviour of concrete; experiments, modelling and analyses. Heron, 37(1), 1–79.

[46] Saenz, L. P. (1964). Equation for the Stress-Strain Curve of Concrete. ACI Journal Proceedings, 61(3), 1229–1235. doi:10.14359/7785.

[47] Johnson, G. R. & Cook, W. H. (1983). A Constitutive Model and Data for Metals Subjected to Large Strains, High Strain Rates, and High Temperatures. Proceedings 7th International Symposium on Ballistics, 19-21 April 1983, The Hague, Netherlands.

[48] Dassault Systèmes. (2022). Using the Johnson–Cook hardening model to define classical metal plasticity, Abaqus Documentation, SIMULIA User Assistance, Dassault Systèmes Simula Corp, Waltham, United States.

[49] Hano, M. M., Hano, S. M. A., & Al-Rawe, H. S. (2025). Examining the Compressive Behavior of SFRC and SCC Using Finite Element and Experimental Methods. Civil Engineering Journal, 11(3), 1132–1144. doi:10.28991/CEJ-2025-011-03-017.

[50] Li, J., Wu, C., & Hao, H. (2015). An experimental and numerical study of reinforced ultra-high performance concrete slabs under blast loads. Materials and Design, 82, 64–76. doi:10.1016/j.matdes.2015.05.045.

[51] ACI PRC 440.2:2023. (2023). Design and construction of externally bonded fiber-reinforced polymer (FRP) systems for strengthening concrete structures—Guide. American Concrete Institute (ACI), Farmington Hills, United States.

[52] Zhang, J., Wu, J., Du, W., Tong, C., Zhu, Z., & Jing, Y. (2023). Residual load-carrying performance of CFRP strengthened RC beam after drop hammer impact. International Journal of Impact Engineering, 175, 104547. doi:10.1016/j.ijimpeng.2023.104547.

[53] Youbi, M. El, Tbatou, T., Kadiri, I., & Fertahi, S. E. D. (2022). Numerical Investigation of HSC Columns Retrofitted by CFRP Materials under Combined Load. Civil Engineering Journal, 8(4), 765–779. doi:10.28991/CEJ-2022-08-04-011.

[54] Alobaidi, H. E., & Al-Zuhairi, A. H. (2023). Structural Strengthening of Insufficiently Designed Reinforced Concrete T-Beams using CFRP Composites. Civil Engineering Journal, 9(8), 1880–1896. doi:10.28991/CEJ-2023-09-08-05.